MECCA

9 771214 082007

THIS ISSUE IS FOCUSED ON RESEARCH IN: DESIGN OF VEHICLES

AIM
Published in the heart of Europe on Czech Technical University in Prague the journal reports about research in the field of internal combustion engines and all other components and aspects of vehicle engineering and vehicle design. The articles from the whole world are welcome.

THE FOLLOWING TOPICS ARE RELEVANT FOR THE JOURNAL MECCA:
- Engines and fuels
- Powertrains (hybrid vehicles, transmissions, ...)
- Chassis
- Vehicle body
- Experimental testing
- Mechatronics
- Vehicle dynamics
- Safety
- Transport Systems
- Electronics in vehicles

PERIODICITY
Three times a year

REVIEW PROCESS
All articles are peer and blind reviewed. At least two reviewers per article.

LANGUAGE
English, bilingual abstract and legends (English/Czech or English/Slovak). Articles coming from non-English speaking coutries are submitted to English correction.

ABSTRACTING AND INDEXING
The journal is part of database of open access publications (DOAJ): https://doaj.org/toc/1804-9338

NEW ADVANCED METHODS IN SIDE CRASH TESTING

JAKUB JELÍNEK
TÜV SÜD Czech, Novodvorská 994/138, +420606613227, jakub.jelinek@tuvsud.com
České vysoké učení technické v Praze, Fakulta strojní, Technická 4, +420606613227, jakub.jelinek@fs.cvut.cz

MILAN RŮŽIČKA
České vysoké učení technické v Praze, Fakulta strojní, Technická 4, milan.ruzicka@fs.cvut.cz

ALŽBĚTA KAFKOVÁ
TÜV SÜD Czech, Novodvorská 994/138, +420725894624, alzbeta.kafkova@tuvsud.com
České vysoké učení technické v Praze, Fakulta strojní, Technická 4, alzbeta.kafkova@fs.cvut.cz

ABSTRACT
This work follows up the previous work [1] regarding the used methodology in the field of passive safety, ie. crash testing. The work is based on experience gained in the Active Lateral Impact Simulator (ALIS) project and describes complete process. The main focus has been given to the fine-tuning of the boundary conditions and loading of the system in order to ensure correct biomechanical loads.
KEYWORDS: CRASH TEST, FINITE ELEMENT METHOD, DESIGN OF EXPERIMENT, BIOMECHANICAL LOADS, DYCOT, ALIS

SHRNUTÍ
Tato práce navazuje na předešlé příspěvky [1] týkající se metodiky v oblasti pasivní bezpečnosti, a zejména crash testování. Tento článek vychází ze zkušenosti získané v rámci projektu bočních nárazů a za použití systému Active Lateral Impact Simulator (ALIS) a popisuje celý postup. Hlavní důraz je kladen na jemné ladění počátečních podmínek a náhradního zatížení působícího na celý systém a k dosažení požadovaných biomechanických kritérií.
KLÍČOVÁ SLOVA: NÁRAZOVÁ ZKOUŠKA, METODA KONEČNÝCH PRVKŮ, NÁVRH EXPERIMENTU, BIOMECHANICKÉ ZATÍŽENÍ, DYCOT, ALIS

1. INTRODUCTION
This work proposes a new advanced approach of combined virtual and physical testing. The main idea is to reduce development time and associated costs by using sled testing which used to be used mainly for physical simulation of frontal crashes. Simulation of side crash in sled environment is not a brand-new topic, but certainly very complex one. This method is not really used on regular basis especially due to predictability issues and low accuracy. This work presents new approach of combination both virtual and physical testing. The whole process starts with full crash simulation, goes through conversion of virtual model to reduced sled model, sled testing and finally is wrapped up with full vehicle crash.

2. MAIN SECTION
2.1 DYCOT
TÜV SÜD Czech has recently invested a large sum to test lab equipped with sled system (catapult) – DYnamic COmponent Testing (DYCOT) [2]. Sled test system consists of sled with grid holes and pusher sled, where all electronics and measurement equipment is mounted as also shown on Figure 1. The pusher sled is being pushed by CSA catapult, equipped with hydraulic piston that can accelerate the sled by up to 90G to total velocity of 100kph with payload of 1000kg. When fully loaded (payload of 5000kg), the piston is capable of accelerating the sled up to 35G. Maximum force is equal to 2.5MN. Maximum acceleration gradient is 14G/ms.

FIGURE 1: DYCOT system during the acceleration of the test sample
OBRÁZEK 1: Systém DYCOT při urychlení zkušebního vzorku

It is usually used for frontal crash test where the occupant safety is being tested. It can also be used for testing of crash-landing of any small airplane that would fit in the lab. Latest addition to the service portfolio is battery pack testing for any battery packs up to 1000kg.

2.2 ALIS

The capabilities of DYCOT sled system have been significantly increased by adding ALIS into serie, right next to the sled platform see Figure 2. It uses up to 6 hydraulic cylinders in order to correctly simulate the door intrusion kinematics during the side crash. It enables one to use only small part of the car

together with dummies and restraint systems and carry out simulation of the side crash with focus on restraint system and biomechanical loads.

The system may seem as a "train of trolleys". The driven sled trolley is mounted to the main hydraulic system that generates the main acceleration pulse. ALIS is mounted on the separate trolley, attached to the sled. The whole structure is shown on Figure 3, where main components are identified. The lateral system consists of additional pneumatic system directly attached to several pneumatic cylinders, ALIS primary structure and control system, linear guiding system and "impact break-in structure".

The main reason for testing is to fine-tune the restraint system in order to get the best biomechanical loading in cheaper and quicker way – on sled. The fact that sled tests with only several trim parts and seats are used instead of fully equipped crash vehicles makes this approach very effective. We are definitely talking about tens of percents.

Door structure deforms and biomechanical loads are reached
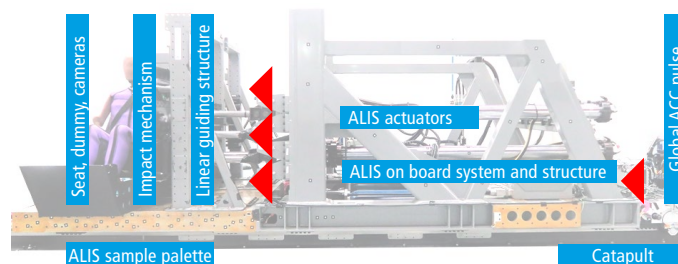
FIGURE 3: DYCOT + ALIS concept
OBRÁZEK 3: Koncept DYCOT + ALIS
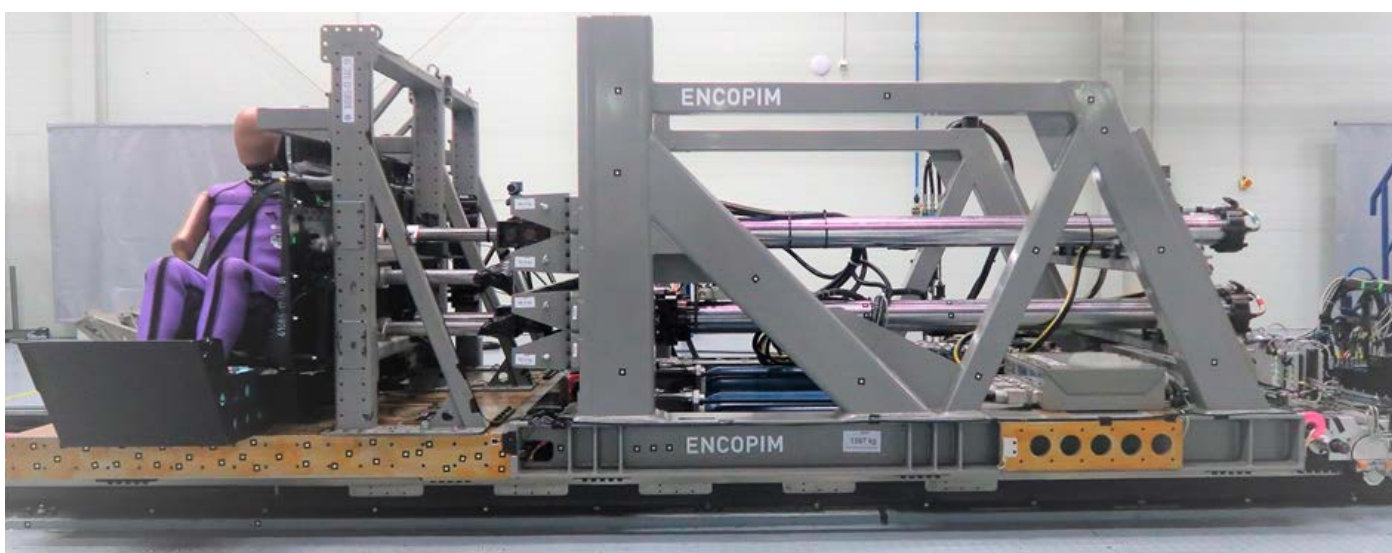
FIGURE 2: Active Lateral Intrusion Simulator (ALIS)
OBRÁZEK 2: Active Lateral Intrusion Simulator (ALIS)

2.3 METHODOLOGY

The whole process starts with FE simulation of full vehicle crash and is shown in Appendix A. It is also very important to mention that usually testing consists of two sets of tests. The first one inputs are based on virtual model and results only and gets the initial recommendations for the first crash test. The second loop inputs are already based on this crash test and requires further development and tuning of ALIS.

2.4 DESIGN OF EXPERIMENT (DOE) [3]

The main objective is to develop a virtual method that would allow reducing full crash into sled crash via ALIS, defining complete ALIS setup and give highly accurate results, while reducing costs.

The DoE method is advanced mathematical method that uses n-dimensional mathematical surface for response values prediction based on combination of input parameters. The aim is to get ideally perfect match between full crash model as given at the beginning of the project and ALIS reduced model.

Amount of input parameters is very often high. One of the ways how to put up with them might be Design of Experiment (DoE) with response surface creation or "step-by-step" iteration with subsequent physical validation as shown in Figure 4. Such method would reduce number of runs and predicts multiple results based on input parameter combinations. Such pulses have to fulfill feasibility criteria of the cylinders and catapult.

2.4.1 PULSE TUNING PROCEDURE

There are several pulses that come into the whole simulation and subsequent physical test. In order to identify and tune pulses two main steps have been chosen. Firstly, contribution of every pulse needs to be determined and secondly chosen pulses have to be fine-tuned in a special manner that will ensure both physical feasibility and biomechanical responses.
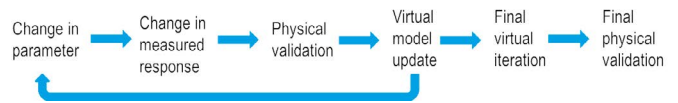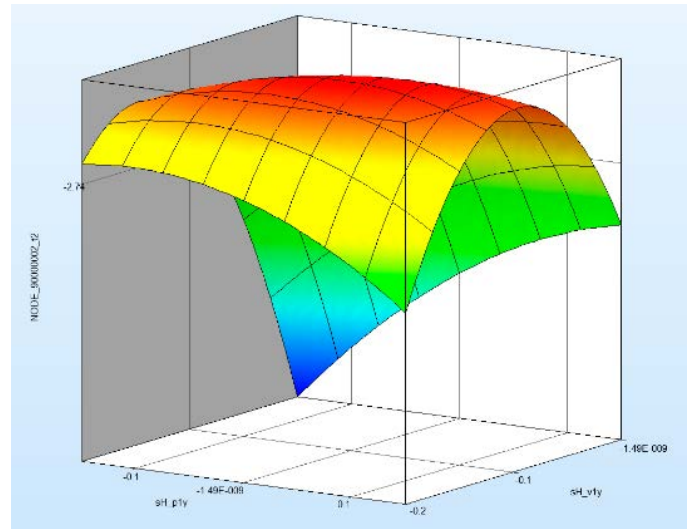
FIGURE 4: DoE response surface (top), step-by-step process (bottom)
OBRÁZEK 4: DoE povrch (nahoře), postupný proces ALIS řešení (dole)

2.4.2 PULSE IDENTIFICATION

Currently there are three hydraulic cylinders available at the ALIS system. One is 120kN and other two are 60kN and therefore three pulses are available. Additional pulse comes from the catapult that represents overall pulses during the side crash. That makes it four pulses available for the first stage of DoE testing. Each pulse has got several parameters such as scale factor for both abscissa and ordinate and also offset values for both abscissa and ordinate. All four pulses have following set of parameters as shown in Figure 5.

		Type	Name	Starting	Init. Range	Minimum	Maximum	Distribution
Variable	▼	🔒	ASD_SY	1.		.85	1.15	(none) ▼
Variable	▼	🔒	ASD_OA	0.		-5.	5.	(none) ▼
Variable	▼	🔒	DBB_SF	1.		.85	1.15	(none) ▼
Variable	▼	🔒	DBB_OA	0.		-5.	5.	(none) ▼
Variable	▼	🔒	DBU_SF	1.		.85	1.15	(none) ▼
Variable	▼	🔒	DBU_OA	0.		-5.	5.	(none) ▼
Variable	▼	🔒	DDD_SF	1.		.85	1.15	(none) ▼
Variable	▼	🔒	DDD_OA	0.		0.	5.	(none) ▼

Design Variables

FIGURE 5: List of design variables
OBRÁZEK 5: Seznam vstupních proměnných

Following variable abbreviations are used:

- ASD_SY – scale factor of sled
- ASD_OA – pulse offset of sled
- DBB_SF – scale factor of actuator at B-pillar bottom
- DBB_OA – pulse offset of actuator at B-pillar bottom
- DBU_SF – scale factor of actuator at B-pillar upper
- DBB_OA – pulse offset of actuator at B-pillar upper
- DDD_SF – scale factor of actuator at door structure
- DDD_OA – pulse offset of actuator at door structure

Since there are 8 variables, the resultant design space will be 8D. Since there is no simple way of illustrating the 8D interactions, we have to go down to 3D visualisation. When always 3 variables are selected and can be switched for any other variable.

All 200 experiments (simulations) have to be run

It has to be pointed out that as there are 8 variables, then 8-dimensional surface will be created based on the responses and hence the complete surface is so complex that cannot be displayed.

ID	Type	Name	Component	Units
90079631		First thorax rib	Compression	mm
90079632		Second thorax rib	Compression	mm
90079633	BAR	Third thorax rib	Compression	mm
90079634		First abdomen rib	Compression	mm
90079635		Second abdomen rib	Compression	mm
90000002		Head acc	Acceleration, velocity	mm ms^{-2} / mm ms^{-1}
90015619		T1 Lower neck acc	Acceleration, velocity	mm ms^{-2} / mm ms^{-1}
90021212	NODE	T4 first thorax acc	Acceleration, velocity	mm ms^{-2} / mm ms^{-1}
90023825		T12 second abdomen acc	Acceleration, velocity	mm ms^{-2} / mm ms^{-1}
90029764		Pelvis acc	Acceleration, velocity	mm ms^{-2} / mm ms^{-1}
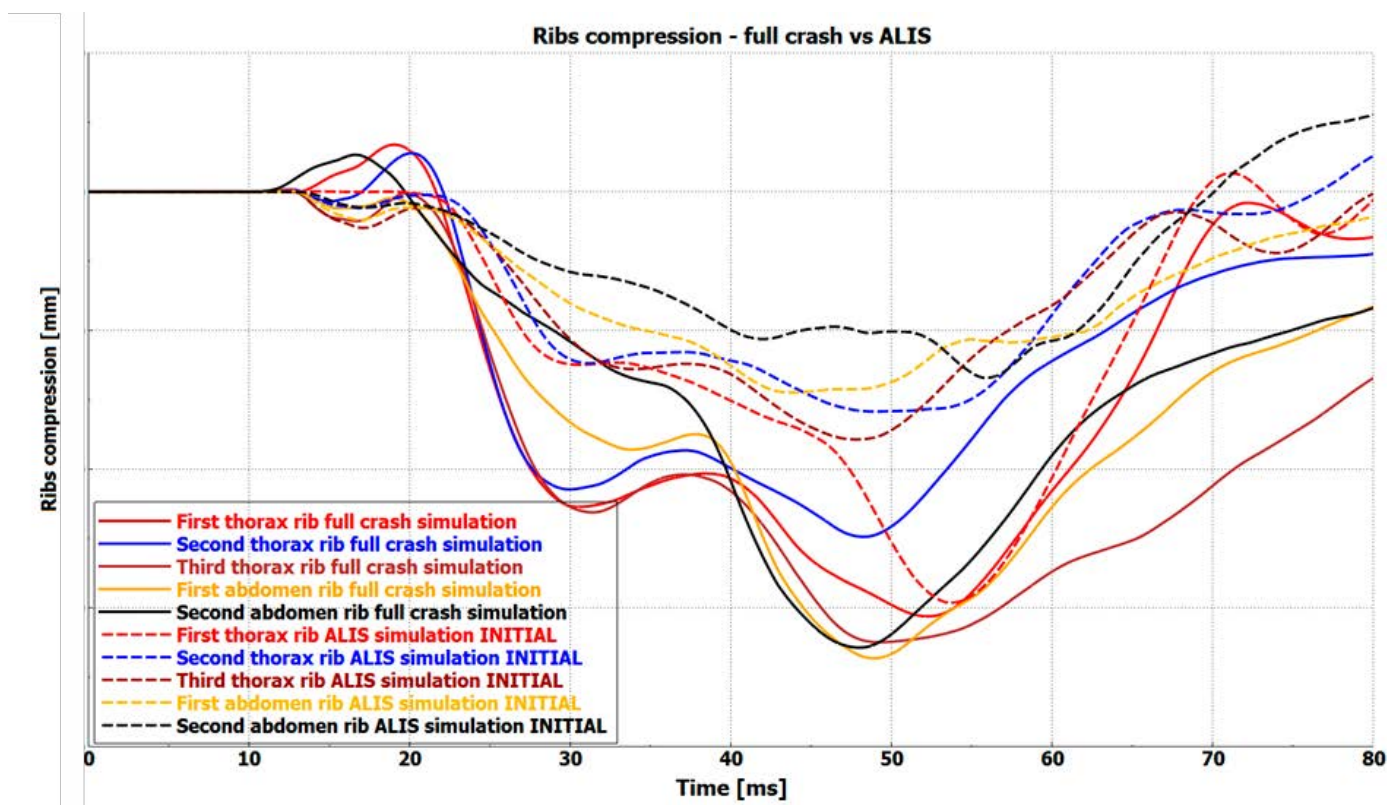
FIGURE 6: Comparison of initial ALIS vs full crash results (ribs)
OBRÁZEK 6: Porovnání úvodních výsledků ALIS s fyzickou zkouškou (žebra)
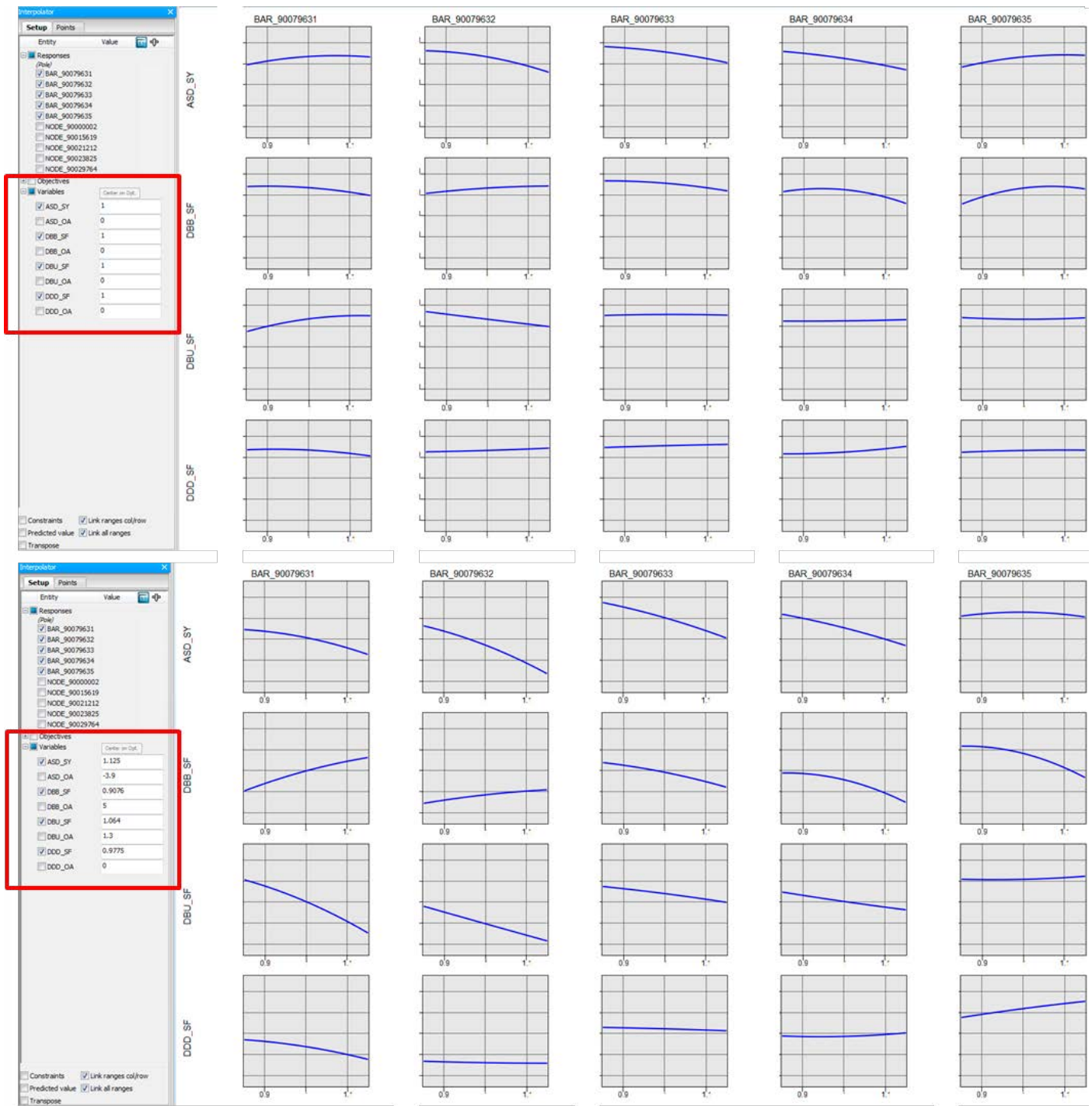
FIGURE 7: The response trends based on initial variable combination (top) and response trends based on update variable combination (bottom)
OBRÁZEK 7: Trendy odezev v úvodním nastavení (nahoře) a trendy založené na upravených parametrech (dole)

2.4.3 RESPONSES

For response surface determination it is necessary to get responses respective to our objectives. Responses are resultants of any measurements such as force, displacement, acceleration, angle, etc. Response list is given by the scope of the sensitivity study.
In all crash simulations, the most important are biomechanical loads that describes the behaviour of a human body during the

crash event. The requirements differ very much from case to case so it is always unique set of criteria that are ideally to be matched. In our pole strike, it is ribs compression. Nowadays, most of the dummies and solvers are able to calculate and/or evaluate these criteria directly via sensors/points of interests. In our case several node and bars have been selected. Nodes are

Label	Name	Value	Initial values
ASD_SY	scale factor of sled	1.02	No
ASD_OA	pulse offset of sled	0	Yes
DBB_SF	scale factor of actuator at B-pillar bottom	1.11	No
DBB_OA	pulse offset of actuator at B-pillar bottom	0	Yes
DBU_SF	scale factor of actuator at B-pillar upper	1.03	No
DBU_OA	pulse offset of actuator at B-pillar upper	0	Yes
DDD_SF	scale factor of actuator at door structure	0.98	No
DDD_OA	pulse offset of actuator at door structure	1	No

used for tuning of controlled trim deformation and its velocity. Simply the velocity and deformation of the trim ensures the same initial conditions as per full crash. Bar then are used for force (shoulder) and displacement (rib compression) evaluation. This metric is the most important for most of the safety crash engineers.

Responses are used for response surface modelling and results evaluation. In our case there are several responses taken into account. They have been chosen according to the requirements of the customer and also EuroNCAP. Responses that have been used are shown in Table 1.

3. RESULTS OF THE VIRTUAL EXPERIMENTS

So far we have been preparing ourselves for the main task. To choose suitable variables from all available sources to achieve the intended responses. Now, when the response surface has been created and validated, the selection of variable that would fit the intended values follows.

The main reason of the virtual experiments is to perform sensitivity analyses that would later give a good knowledge of the system behaviour. This is particularly useful during the physical testing, when quick response to the current behaviour and recommendation of the next steps is highly expected and
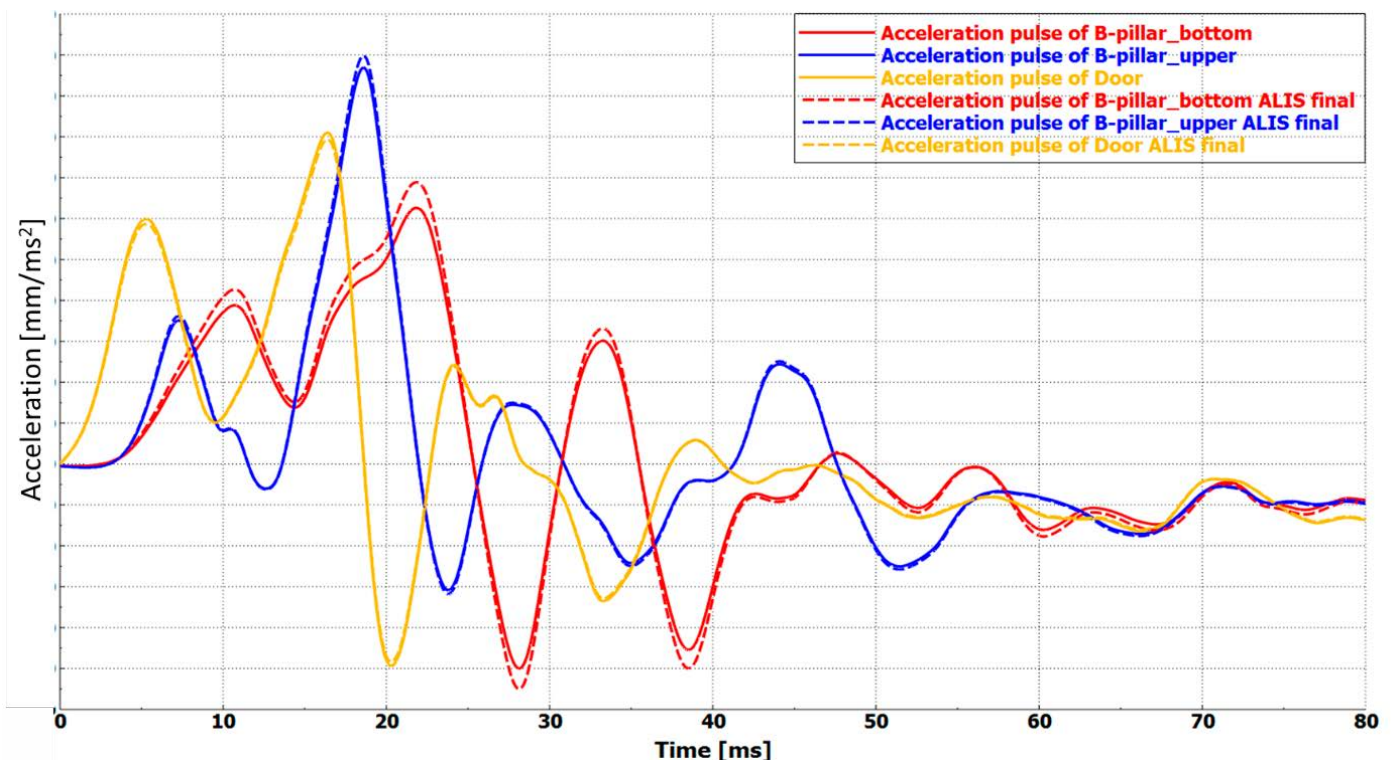
FIGURE 8: Comparison of initial and final ALIS pulses
OBRÁZEK 8: Porovnání úvodních a finálních pulsů ALIS

there is no time for further simulations. In order to get ideal pulse configurations for respective biomechanical responses, it is necessary to set the target. EuroNCAP assessment is based on scoring system of the maximal biomechanical loads.

For illustration there is a comparison of initial ALIS run, with all variables equal to 1, and full crash model shown on Figure 6. The match is not ideal one at the moment and our goal is to get better match. Hence there has to be an update done of some or all available pulses (scale factor or offset). The suitable variable combinations can be found by user to achieve his requirements. LS-OPT can easily predict response values based when one changes the input variables as indicated on Figure 7.

This is exactly the way how to better understand mutual interaction between input variables and responses.

In our case, when the five ribs are of interest, we get desired response with following variables written in Table 2.

As these values are predicted, another testing run has to be to verify the suitability. Updated three pulses for ALIS and one for sled are shown on Figure 8.

Updated ALIS results of dummy biomechanical criteria compared to full crash data are displayed on Figure 9.

The comparison shows rather good match of both simulation approaches. Reduced model is and always will be only approximation and can only get close to the full crash simulation model. Four pulses with reasonable match, which is usually considered within deviation of 10%, to the full crash model have been found and hence the first objective is complete. Secondary objective was to get a good knowledge of the system behaviour and it has also been done. It will become very useful in upcoming testing.

4. CONCLUSION

This paper has shown how to handle ALIS project within the virtual part. The main objective (pulses identification) has been achieved. Controlled pulses have become input parameters into the physical sled test. It is very important to get a good knowledge of the whole system behavior and how biomechanical responses are affected by variation of input as this helps the tuning procedure during early physical testing. Without it, one would not be able to recommend further steps to improve the results accuracy.

Future work is to cover the last remaining part and it is the physical testing and results validation.

LIST OF NOTATIONS AND ABBREVIATIONS

ALIS – Active Lateral Impact Simulator
ASD_SY – scale factor of sled
ASD_OA – abscissa offset
DBB_SF – B-pillar bottom scale factor
DBB_OA – B-pillar bottom abscissa offset
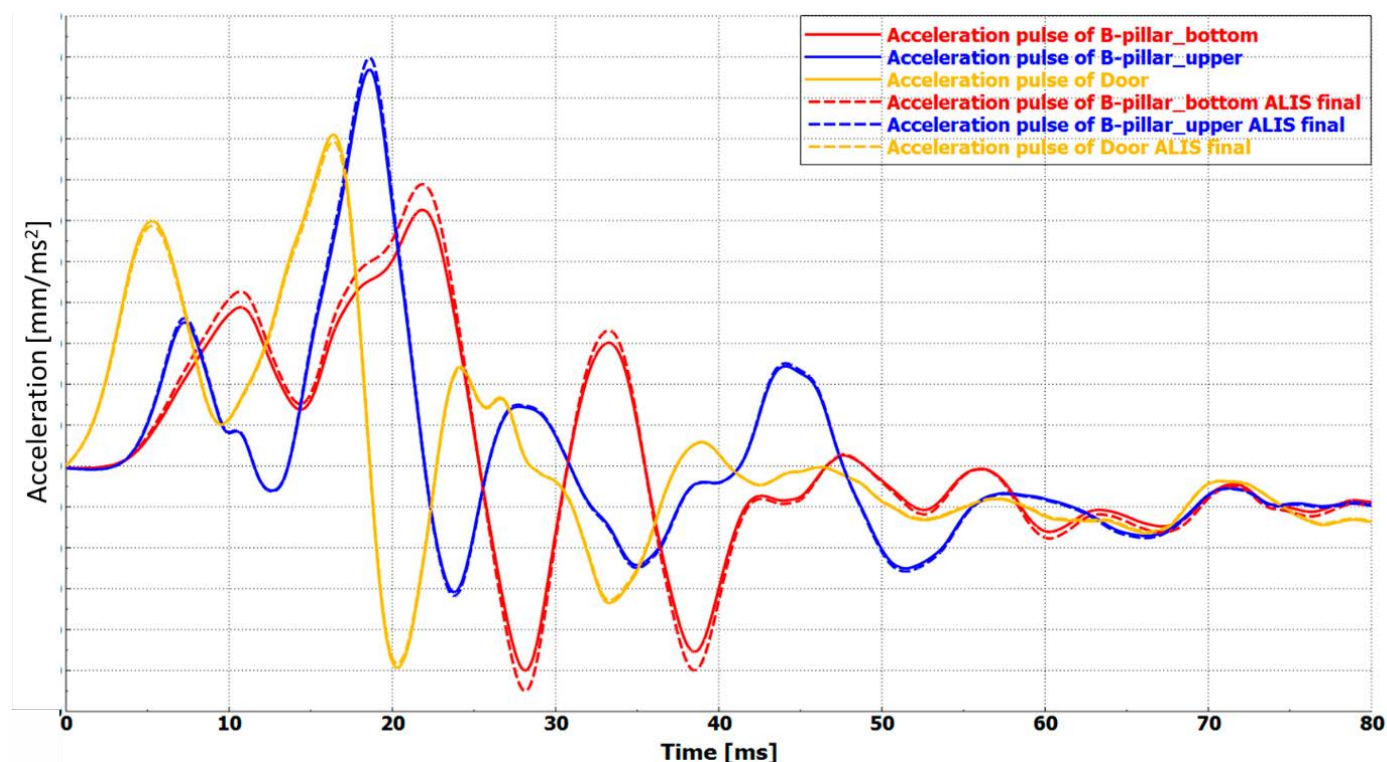
FIGURE 8: Comparison of initial and final ALIS pulses
OBRÁZEK 8: Porovnání úvodních a finálních pulsů ALIS

DBU_SF – B-pillar upper scale factor
DBU_OA – B-pillar upper abscissa offset
DDD_SF – door scale factor
DDD_OA – door abscissa offset
DoE – design of experiment
DYCOT – Dynamic Component Testing
ENCAP – European New Car Assessment Programme

REFERENCES

[1] Jelinek J., Růžička M., Kalinský M. Advanced Methods in Crash Safety Testing, 56th Conference on Experimental Stress Analysis Proceedings 2018, ISBN 978-80-270-4062-9

[2] Šotola M., 2016. DYCOT presentation, TÜV SÜD Czech, pages 3-7

[3] Jelinek J., Růžička M. Advanced methods in crash safety testing, 24th Workshop of Applied Mechanics 2018, ISBN 978-80-01-06453-5

APPENDIX A – METHODOLOGY

Output is to be biomechanical loads, intrusion and kinematics of important structural parts such as doors, A- and B-pillars.
Size reduction of FE model comes next. The most important outcome of this phase is determination of the ALIS settings. This includes number of cylinders used, their timing and also design of the impact structure. Amount of input parameters is countless. Other two phases are related to the physical testing.
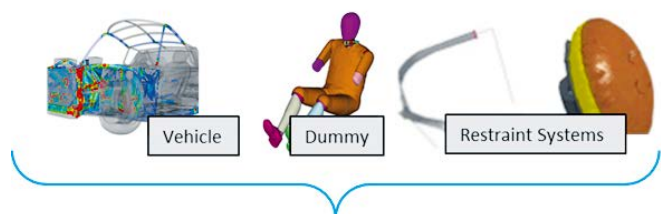
Full Car FE Simulation
Output:
Biomechanical Loads
Intrusion
Kinematics

Model Reduction
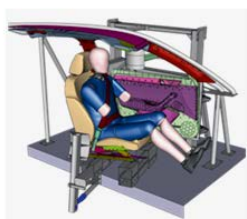
Size-Reduced FE Simulation
Output:
Number of cylinders
Cylinder positions
Force distribution (shape and magnitude)
Impact structure design

ALIS Parameters Application

Reduced Physical Crash Test
Output:
Biomechanical Loads

Correlation

Physical Crash Test
Output:
Biomechanical Loads

FIGURE 10: Real crash to ALIS reduction procedure [3] (Courtesy of Škoda Auto)
OBRÁZEK 10: Proces redukce z reálného crash testu po ALIS [3] (S laskavým dovolením Škoda Auto)

SOFTWARE FOR THE DESIGN OF GEARING WITH AN ASYMMETRIC PROFILE

ONDŘEJ MILÁČEK

CTU in Prague, Department of Automotive, Combustion Engine and Railway Engineering, Vehicle Center of Sustainable Mobility, ondrej.milacek@fs.cvut.cz

ABSTRACT

This article is a continuation of previously published articles. This paper briefly describes the positive and negative qualities of asymmetric gearing from the point of view of loading conditions applied at the gearset, and the development and latest update of the software for designing this special involute gearing. The precise profile of the manufacturing tool is also described. All display options, and the option of gear mesh animation using this program, is shown. All equations necessary for the gearing geometry description, and a special approach with respect to x-shift coefficients distribution, are also mentioned in this paper.

KEYWORDS: ASYMMETRIC, INVOLUTE, GEARING, EXTERNAL, ANIMATION, TIP CHAMFER, PROTUBERANCE, RACK

SHRNUTÍ

Tento článek je pokračováním dříve publikovaných článků. Stručně popisuje pozitivní a negativní vlastnosti asymetrického ozubení z pohledu zátěžných stavů působících na ozubené soukolí, a vývoj a poslední změny nového softwaru určeného pro návrh tohoto speciálního evolventního ozubení. Detailní profil výrobního nástroje je rovněž zmíněn. Prezentovány jsou všechny možnosti zobrazení a možnosti nastavení animace záběru ozubení, které tento program umožňuje. Zmíněny jsou také veškeré rovnice, popisující geometrii ozubení a zvláštní přístup k rozdělení koeficientů jednotkového posunutí x.

KLÍČOVÁ SLOVA: ASYMETRICKÉ OZUBENÍ, INVOLUTA, OZUBENÍ, VNĚJŠÍ, ANIMACE, SRAŽENÍ HRANY NA HLAVĚ ZUBU, PROTUBERANCE, VÝROBNÍ HŘEBEN

1. INTRODUCTION

The issue of involute gearing geometry is a topic well-covered by specialist literature. It is very important to connect the influence of the production technology. Modern technologies allow the fine-tuning of the profile using CNC milling, electrical discharge machining (EDM) or grinding machines. In this article, the gearing profile is created purely by a trochoidal milling method with a cutting tool (rack). This rack profile also includes the tip chamfer and the protuberance. The gearing profile can be asymmetric.

2. NOMENCLATURE AND USAGE OF ASYMMETRIC GEARING

Initially, the side (flank) nomenclature should be defined. When driving a car, the power is transmitted at the "drive" flank; with engine (ICE) braking (going downhill without the gas pedal pressed), power is transmitted from the wheels to the engine via the "coast" flank of the teeth. In the case of a passenger car, load conditions at both tooth flanks can be very different. This important difference is caused by ICE turbocharging (torque increase). This means that one tooth flank is used much more often and with higher loading torque than the opposite one. This situation is depicted in Figure 1. The recorded torque during a real test drive of a passenger car is used as input data. These measured torque values are then sorted into "load levels". At each load level is then calculated an average torque and number of occurrences – the "load level spectrum". The effect of this whole loading spectrum on the gearset can then be transformed into loading with constant "equivalent" torque M_e, which causes the same damage as the spectrum while undergoing the same number of cycles n. The exact procedure of its processing is described in [1].

Figure 1 depicts a typical situation for a passenger car where the tooth flank at the coast side is loaded only with the torque value of 49% and only for 35% of loading cycles in comparison with the drive flank. In the case of lorries, loading torque at the coast

side increases due to usage of an engine brake or retarder, so there are comparable loading conditions at both flanks. For this reason, a symmetric gearing profile makes sense is in this case.
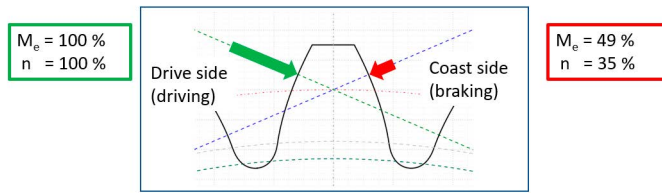
FIGURE 1: Loading conditions of the passenger car at both tooth flanks while driving and braking by ICE.
OBRÁZEK 1: Zátěžné stavy v osobním vozidle na obou stranách zubu, pohon a brzdění motorem

From the point of view of gearing durability, a symmetric profile in the case of passenger cars is not ideal. One side is always either overloaded or has excessive durability, particularly from the perspective of Hertzian (contact) stresses, which affect pitting formation. To optimize the durability at both tooth sides according to loading conditions, it is useful to reduce the contact stress on the drive side. This reduction can be achieved using an asymmetric gearing profile. This means that the most important parameter of the rack profile – angle α_n (α_{P0}) – is not same for both sides.

3. RELIABILITY COMPUTATION METHODOLOGY FOR ASYMMETRIC GEARING

Analytically, the Hertzian stress at a single tooth contact can be computed using a formula (1), where both osculation radii of touching bodies are known. In the case of a helical gearset, these bodies are cylinders with radii $\rho_{1,2}$.

$$\sigma_H = \sqrt{\frac{F_n}{\pi \cdot b} \cdot \frac{E}{2 \cdot (1 - \nu^2)} \cdot \left(\frac{1}{\rho_1} + \frac{1}{\rho_2}\right)} \tag{1}$$

where: σ_H Hertzian stress
         F_n normal force
         b facewidth
         E Young's modulus of elasticity
         ν Poisson's ratio
         $\rho_{1,2}$ osculation radii

For involute gearing, the values of these osculation radii are dependent on its geometry. The situation is depicted in Figure 2.

This figure shows that these values are given, based on the involute geometry, as

$$\rho_{1,2} = r_{w\,1,2} \cdot \sin \alpha_{tw} \tag{2}$$

where: $\rho_{w1,2}$ working pitch radii of both gearwheels
         α_{tw} working transverse pressure angle

This means that the contact stress can be reduced while maintaining the gearset's major dimensions only by increasing the working transverse pressure angle α_{tw}. It is also clear that these osculation radii are much bigger at the drive side (blue) than at the coast side (green).
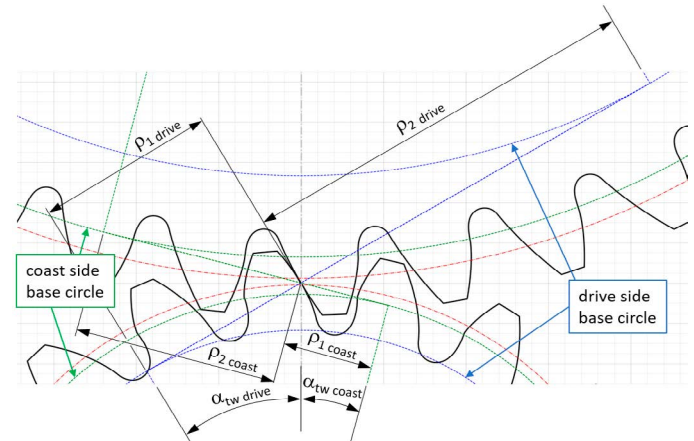
FIGURE 2: Osculation radii of involute gearset for single tooth contact in the mesh point.
OBRÁZEK 2: Oskulační poloměry (poloměry křivosti) evolventního ozubení při jednopárovém záběru ve valivém bodě.

Unlike for symmetric gearing, no standards yet exist for calculation of the lifetime of involute gearing with an asymmetric profile. For this reason, FEM simulation must be used firstly for symmetric gearing. These results must be compared with the stress obtained from a standardized calculation. Included in this calculation are all meshing and loading conditions using necessary coefficients (e.g. software KissSoft). By comparing both these results, recalculation coefficients are defined – see formula (3) for contact stress and formula (4) for root bending stress at each gearwheel.

$$k_{H\,FEM} = \frac{\sigma_{H\,KissSoft}}{\sigma_{H\,FEM}} \tag{3}$$

$$k_{F\,FEM_{1,2}} = \frac{\sigma_{F\,KissSoft_{1,2}}}{\sigma_{F\,FEM_{drive\,side_{1,2}}}} \tag{4}$$

These coefficients are then used for backward recalculation of FEM results of asymmetric gearing to be comparable with
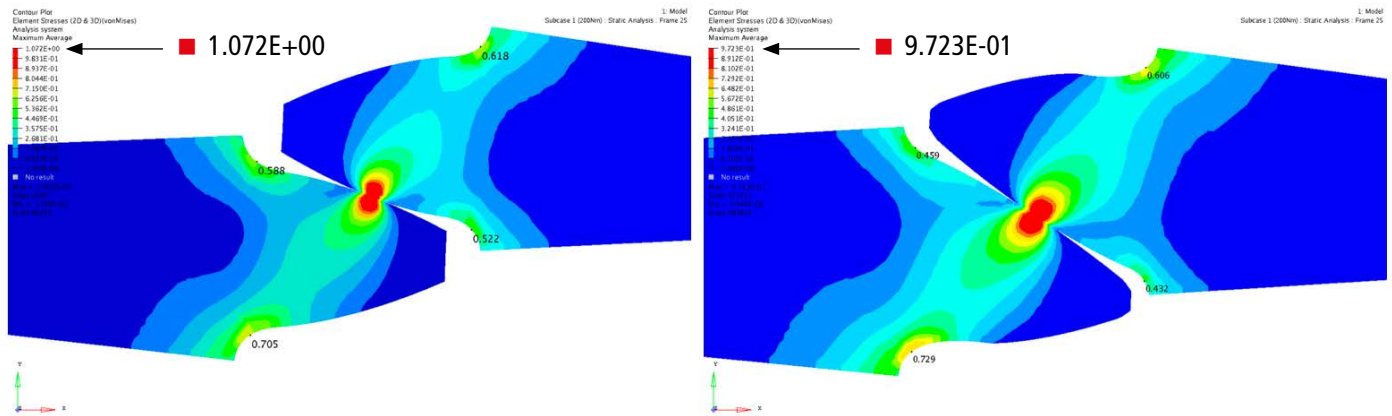
FIGURE 3: Example of FEM analysis of symmetric and asymmetric gearing, both profiles were designed using developed program.
OBRÁZEK 3: Příklad FEM analýzy symetrického a asymetrického ozubení, oba profily byly vytvořeny s pomocí popisovaného programu

symmetric gearing results. To obtain the asymmetric gearing profile as an input for FEM analysis, the software described in the following chapter was developed.

The output from this program is also very important. The final gearset design from this program is further used for the creation of a 3D CAD model (e.g. to Catia using a function "Design Table") to create an input file (*.stp or *.igs) for an FEM solver. To be able to transfer the geometry further there is an option of saving all necessary parameters and coordinates of all calculated points into a "*.csv" file. An important advantage of this program is that the output is a chosen amount of calculated points, so the change of the design in 3D is then very fast – just the loading of a new (rewritten) design table in MS Excel.

The following Figure 3 depicts an example of gearset FEM analysis. It's a comparison of symmetric and asymmetric variants of a gearset. The decrease in the contact pressure by the same load (torque) for the asymmetric variant is approx. 9.3%. Values of maximum stress (von Mises [GPa]) are enlarged to be readable. On the other hand, asymmetric profile (higher pressure angle) also has one negative consequence – the increase in radial forces, which cause higher loading on the bearings.

4. STANDARD APPROACH TO SYMMETRIC INVOLUTE GEARING DESIGN

When designing the macrogeometry of a symmetric gearset according to applicable standards (e.g. DIN 3990:1987, Method B in KissSoft), all input parameters must be determined. In the next step, the sum of required x-shift coefficients x_Σ for the gearset can be calculated using equation (5).

$$x_\Sigma = x_1 + x_2 = \frac{z_1 + z_2}{2 \cdot tg\, \alpha_n} \cdot (inv\, \alpha_{tw} - inv\, \alpha_t) \quad (5)$$

where: $x_{1,2}$ x-shift coefficients
          $z_{1,2}$ number of teeth
          $\alpha_n\,(\alpha_{P0})$ normal (tool) pressure angle
          α_t transverse pressure angle
          α_{tw} working transverse pressure angle

This value of x_Σ is calculated with the condition of no backlash, and is then divided among each gearwheel according to loading or geometrical conditions and demands on the wheels. Finally, needed backlash is implemented to the final gear shape by the given standard (e.g. DIN 3967). An example of such gearing including the backlash can be seen in Figure 4.
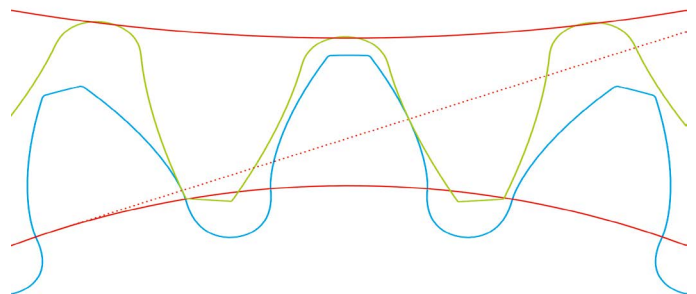
FIGURE 4: Example of the gearset appearance including the backlash designed in KissSoft
OBRÁZEK 4: Ukázka vzhledu ozubeného soukolí (včetně vůle), navrženého v programu KissSoft

5. ASYMMETRIC INVOLUTE GEARING GEOMETRY DESCRIPTION

In the case of a symmetric profile (rack), the tooth thickness is simply divided into two identical halves. In the case of asymmetric gearing, the situation is different. Figure 5 shows

the situation in the transverse plane during manufacture, i.e. the mesh of the tool (rack) with a gearwheel. All values with the symbol "0" are related to a tool. The tool geometry description follows. A basic parameter is the thickness at tool reference plane s_{t0}, which equals half of the transverse pitch p_{t0}, as in the case of a symmetric version.

$$s_{t0} = \frac{p_{t0}}{2} = \frac{\pi \cdot m_t}{2} \tag{6}$$

where: m_t transverse module

This tool thickness is a sum of partial tool thicknesses at both sides (drive and coast)

$$s_{t0} = s_{t0\ drive} + s_{t0\ coast} \tag{7}$$

Furthermore, the asymmetry ratio "A" depending on the transverse profile angles can be defined as the ratio of both these thicknesses

$$A = \frac{s_{t0\ drive}}{s_{t0\ coast}} = \frac{\tan \alpha_{t\ drive}}{\tan \alpha_{t\ coast}} \tag{8}$$

For symmetric gearing this value is $A = 1$. For asymmetric gearing there is standardly higher value of the profile angle α_t on the drive side. From this reason also the thickness on the drive side is higher than on the coast side and thus the asymmetry ratio is standardly $A > 1$.

$$s_{t0\ drive} = s_{t0} \cdot \frac{A}{1+A}\quad , \quad s_{t0\ coast} = s_{t0} \cdot \frac{1}{1+A} \tag{9}$$

Regarding the tooth profile, the rack shift must be considered. If the x-shift coefficient is equal to zero, the tooth thickness s_t at the reference diameter d is the same as the thickness of the tool (gap) s_{t0}. If the rack is in a general position, i.e. shifted about the distance of "$x.m_n$" as depicted in Figure 5, tooth thicknesses at reference diameter on both sides are still divided in same ratio A and their values are

$$s_{t\ drive} = s_{t0\ drive} + x \cdot m_n \cdot \tan \alpha_{t\ drive} =$$
$$= s_{t0\ drive} + x \cdot m_t \cdot \tan \alpha_{n\ drive} \tag{10}$$

and

$$s_{t\ coast} = s_{t0\ coast} + x \cdot m_n \cdot \tan \alpha_{t\ coast} =$$
$$= s_{t0\ coast} + x \cdot m_t \cdot \tan \alpha_{n\ coast} \tag{11}$$

where: m_n normal module
       β helix angle
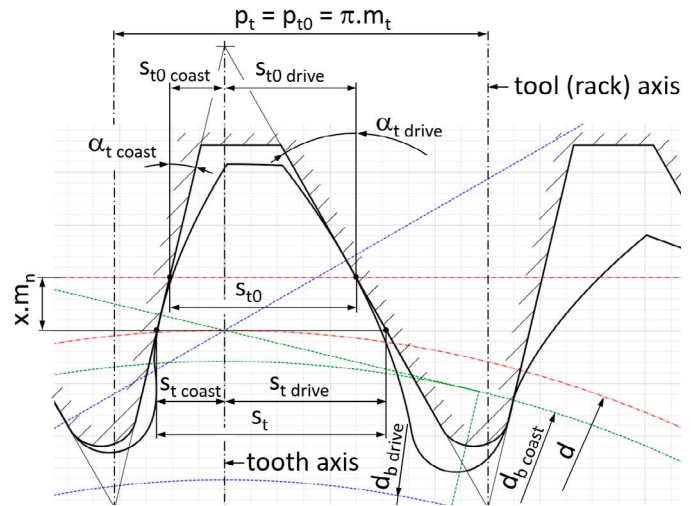
FIGURE 5: Situation in transverse plane while manufacturing of asymmetric gearing
OBRÁZEK 5: Situace v tečné rovině při výrobě asymetrického ozubení

To be able to derive a formula for a needed sum of x-shift profile coefficients for the case of asymmetric gearing without a backlash, the basic condition of correct mesh must be used, see formula (12). The meaning is that the sum of tooth thicknesses of mating gears at their working pitch diameters must remain the transverse pitch.

$$p_{tw} = s_{tw1} + s_{tw2} \tag{12}$$

These working pitch diameters can be calculated purely from the kinematic ratio using of number of teeth as (13)

$$r_{w1} = \frac{a_w}{1 + \frac{z_2}{z_1}}\quad , \qquad r_{w2} = \frac{a_w \cdot \frac{z_2}{z_1}}{1 + \frac{z_2}{z_1}} \tag{13}$$

For a symmetric gearing, these thicknesses $s_{tw1,2}$ can be computed using formula (14) as

$$s_{tw\ 1,2} = d_{w\ 1,2} \left(\frac{s_{t\ 1,2}}{d_{1,2}} + inv\ \alpha_t - inv\ \alpha_{tw} \right) ,$$

$$inv\ \alpha = \tan \alpha - \alpha\ [rad] \tag{14}$$

where working transverse pressure angle α_{tw} can be calculated using formula (15) as

$$\alpha_{tw} = \arccos \left(\frac{a_n}{a_w} \cdot \cos \alpha_t \right) \tag{15}$$

where: $a_n = r_1 + r_2$ nominal center distance
       $a_w = r_{w1} + r_{w2}$ working (real) center distance

For an asymmetric profile, these thicknesses $s_{tw1,2}$ can also be computed, using formula (14), but separate for each tooth side. Radii must be used instead of diameters, see formulas (16) and (17).

$$s_{tw\ drive\ 1,2} = r_{w\ 1,2} \left(\frac{s_{t\ drive\ 1,2}}{r_{1,2}} + inv\ \alpha_{t\ drive} - inv\ \alpha_{tw\ drive} \right) \tag{16}$$

$$s_{tw\ coast\ 1,2} = r_{w\ 1,2} \left(\frac{s_{t\ coast\ 1,2}}{r_{1,2}} + inv\ \alpha_{t\ coast} - inv\ \alpha_{tw\ coast} \right) \tag{17}$$

By the summing of these two parts, total tooth thickness can be defined on working pitch diameters $d_{w1,2}$ for both gearwheels, see formula (18)

$$s_{tw\ 1,2} = s_{tw\ drive\ 1,2} + s_{tw\ coast\ 1,2} \tag{18}$$

The aim is to determine needed sum of both x-shift coefficients. From this reason these values $x_{1,2}$ must be used for description of the thicknesses $s_{tw1,2}$, see equation (19).

$$\begin{aligned} s_{tw\ 1,2} = r_{w\ 1,2} \Bigg(\frac{m_t \cdot \pi}{2 \cdot r_{1,2}} + \frac{m_t \cdot x_{1,2}}{r_{1,2}} \cdot (\tan \alpha_{n\ drive} + \tan \alpha_{n\ coast}) + inv\ \alpha_{t\ drive} \\ - inv\ \alpha_{tw\ drive} + inv\ \alpha_{t\ coast} - inv\ \alpha_{tw\ coast} \Bigg) \end{aligned} \tag{19}$$

The sum of these two thicknesses follows, see formula (20).

$$\begin{aligned} s_{tw\ 1} + s_{tw\ 2} = \frac{m_t \cdot \pi}{2} \cdot \left(\frac{r_{w1}}{r_1} + \frac{r_{w2}}{r_2} \right) + (x_1 + x_2) \cdot m_t \cdot \frac{r_{w1}}{r_1} \cdot (\tan(\alpha_{n\ drive}) + \tan(\alpha_{n\ coast})) + (r_{w1} + r_{w2}) \\ \cdot (inv\alpha_{t\ drive} - inv\alpha_{tw\ drive} + inv\alpha_{t\ coast} - inv\alpha_{tw\ coast}) \end{aligned} \tag{20}$$

The value of $(r_1 + r_2)$ can be substituted using formula (21). Values of appropriate mesh angles α_t and α_{tw} can be taken either from drive or coast side because their ratio used in formula (21) remains same for both of them.

$$r_{w1} + r_{w2} = a_w = a_n \cdot \frac{\cos \alpha_{t\ drive}}{\cos \alpha_{tw\ drive}} = \frac{(z_1 + z_2) \cdot m_t}{2} \cdot \frac{\cos \alpha_{t\ drive}}{\cos \alpha_{tw\ drive}} \tag{21}$$

Transverse pitch p_{tw} at working pitch diameters $d_{w1,2}$ can be computed using formula (22) as

$$p_{tw} = p_t \cdot \frac{d_w}{d} = \pi \cdot m_t \cdot \frac{d_w}{d} = \pi \cdot m_t \cdot \frac{\cos \alpha_{t\ drive}}{\cos \alpha_{tw\ drive}} = \pi \cdot m_t \cdot \frac{\cos \alpha_{t\ coast}}{\cos \alpha_{tw\ coast}} \tag{22}$$

Now it is possible to put all needed formulas into the equation (12). The final result of this condition is the desired sum of x-shift coefficients $x_1 + x_2$ of both gearwheels, see formula (23).

$$x_\Sigma = x_1 + x_2 = \frac{(z_1 + z_2) \cdot (inv\alpha_{tw\ drive} - inv\alpha_{t\ drive} + inv\alpha_{tw\ coast} - inv\alpha_{t\ coast})}{2 \cdot (\tan \alpha_{n\ drive} + \tan \alpha_{n\ coast})} \tag{23}$$

As it was already mentioned, value of x_Σ resulting from the equation (23) is derived for the condition of theoretical mesh with no backlash between tooth flanks. Similarity with the equation (5) is obvious at the first glance. The only difference lays in the fact, that appropriate expressions are used separately for each tooth side, instead of one value identical on both sides as for symmetric profile. One of these two values $x_{1,2}$ must be set and the second one is then calculated from x_Σ.

6. DEPICTION OF THE GEARSET INCLUDING THE BACKLASH

For assuring of correct gearset function some minimal backlash is needed between tooth flanks while meshing. To be able to determine and depict this circumferential transverse backlash j_t we must focus again on working pitch diameters $d_{w1,2}$ where thicknesses of mating gears are important. On these diameters transverse working pitch p_{tw} remains same as for the case of meshing without a backlash and can be defined using formula (22). Teeth thicknesses of both gears can be computed using formula (19). Fundamental condition for meshing without a backlash expressed by the equation (12) then changes to the equation (24), where circumferential backlash j_t is already considered.

$$p_{tw} = s_{tw1} + s_{tw2} + j_t \qquad (24)$$

Formula (24) can then be used to express the circumferential transverse backlash j_t as

$$j_t = p_{tw} - s_{tw1} - s_{tw2} \qquad (25)$$

From this formula (25) it is clear, that the sum of both tooth thicknesses $s_{tw1,2}$ must be smaller than for the case without clearance. These thicknesses are influenced by the values of x-shift coefficients. This means that for case including the backlash the equation (23) cannot be used. When considering a real case including the backlash, both values of $x_{1,2}$ must be entered and resulting transverse backlash j_t can be then calculated.

More important than circumferential transverse backlash j_t is the normal one j_n. In the case of asymmetric gearing, the same formula is used as for a symmetric profile, but relevant angles differ at both sides, see formula (26).

$$j_{n\ drive} = j_t \cdot \cos\alpha_{tw\ drive} \cdot \cos\beta_w$$
$$ \qquad (26) $$
$$j_{n\ coast} = j_t \cdot \cos\alpha_{tw\ coast} \cdot \cos\beta_w$$
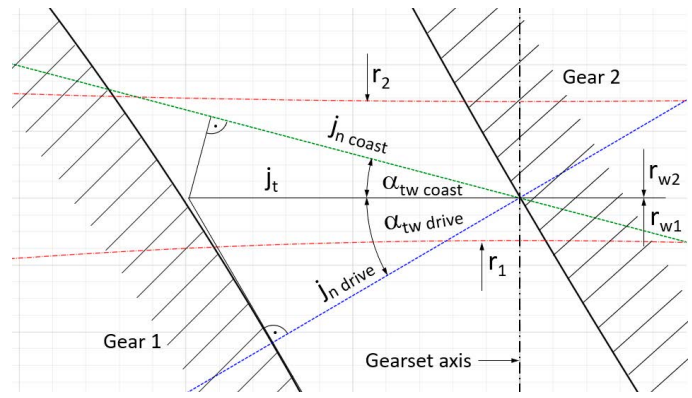
FIGURE 6: Recalculation from circumferential transverse backlash to normal backlash - detail
OBRÁZEK 6: Přepočet obvodové vůle v tečné rovině do roviny normálové
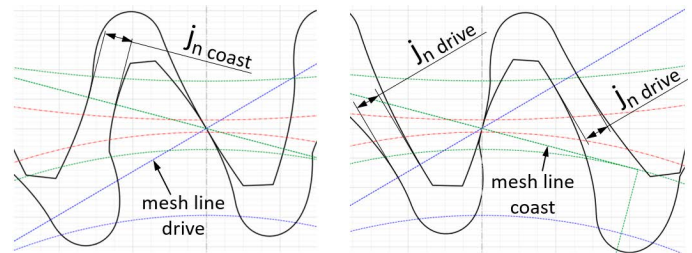
FIGURE 7: Normal backlash j_n between coast/drive flanks while drive/coast flanks meshing (left/right).
OBRÁZEK 7: Normálová vůle j_n mezi coast/drive čely během drive/coast záběru (vlevo/vpravo).

The situation while recalculating backlashes is depicted in detail in Figure 6. This figure applies only for spur gearing, in the case of helical gearing the influence of helix angle β_w cannot be depicted in transverse plane. Nevertheless, in equations (26) it is included, so computed values of j_n shown in the program are correct.

While meshing of drive flanks, the backlash between coast flanks appears and conversely, see Figure 7. Normally the drive side is the more important one and has a higher value of mesh angle than the coast one. For this reason, backlash at the coast side is standardly also higher, see Figure 6.

7. APPROACH OF THIS PROGRAM, ITS APPEARANCE AND FUCTIONS

This software was developed in the Python programming software. Units of all used and displayed values are [mm]. The KissSoft program served as an example of its appearance. One of the first versions is depicted in Figure 9. A very important difference in comparison with KissSoft lies in the approach to backlash in the gearset.

When designing a gearset, input parameters must be given. This is normally the ratio (number of teeth), working center distance and maximum addendum diameters restricted by space requirements.
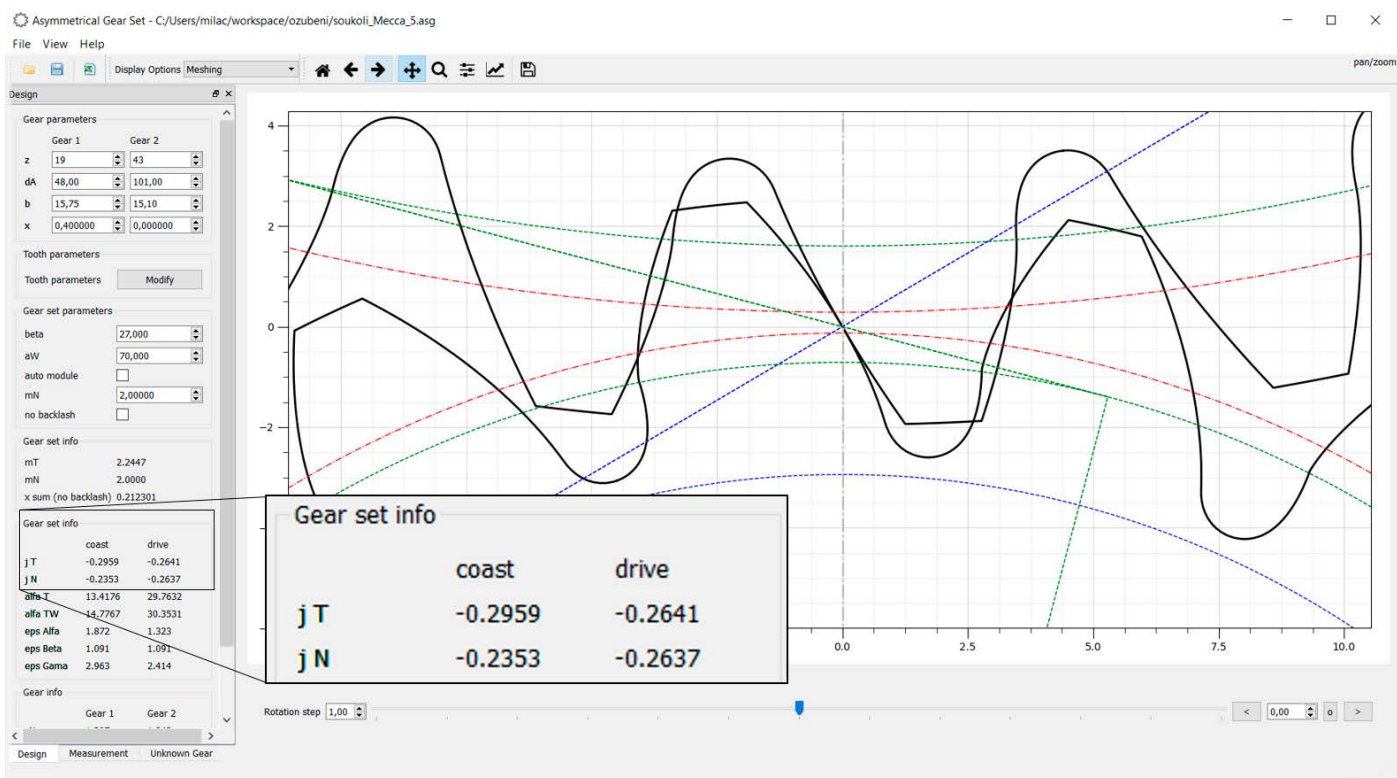
FIGURE 8: Example of the gearset with negative backlash value - nonsense
OBRÁZEK 8: Příklad ozubeného soukolí se zápornou hodnotou vůle - nesmysl

Subsequently, tooth profile (mesh angle) and helix angle are determined. The result of the gearset macrogeometry design is the sum of profile shift x_Σ for the condition of no backlash.
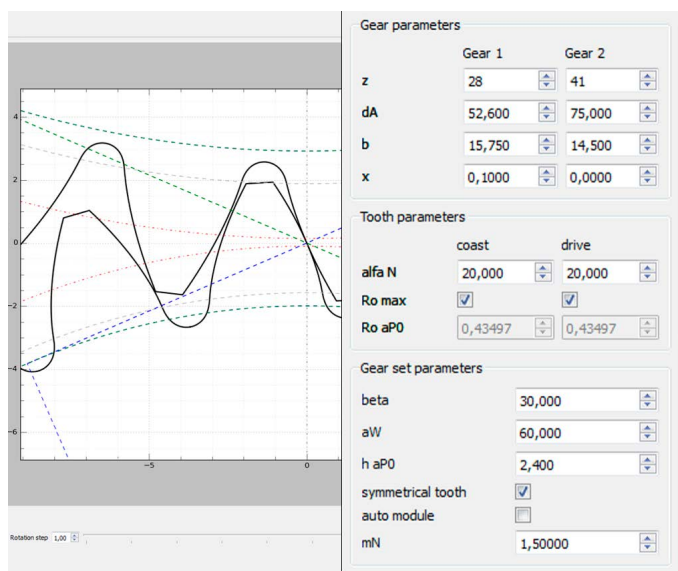
FIGURE 9: Appearance of the program initial version for depicting symmetric and asymmetric gearing – example of a gear mesh
OBRÁZEK 9: Vzhled počáteční verze programu, zobrazující symetrické i asymetrické ozubení - příklad zubů v záběru soukolí

Real tooth profiles (values of x- shift coefficients) are subsequently changed according to related standards (e.g. DIN 3967) to reach desired backlash, which is crucial for correct gearset function.

In the case of the program described in this contribution, x_Σ can be either calculated directly using formula (23) for the condition of no backlash or can be entered manually, separately for each gear including the x-shift coefficients. An exception to this are common parameters of both gears (e.g. helix angle). Gearwheel profiles are directly depicted including the backlash (if possible) and all needed parameters are calculated. Example of such situation is depicted in Figure 7. Indeed, the situation when negative backlash appears can occur, see Figure 8. Of course, in reality negative backlash is nonsense, its value must be always positive. From this reason it is very important to check backlash values. Their values are enlarged in Figure 8.

Development of this software was quite demanding. In the following text its appearance and parameters at given stages are depicted and described.

The first version is depicted in Figure 9. At this stage it was possible to set only the basic parameters of the rack. These input parameters are mentioned in the following Table 1. Furthermore, for the manufacturing of both gears only one (identical) cutting tool was considered. This issue can cause the tip – root interference. Besides all necessary parameters, there is

Gear parameters

	Gear 1	Gear 2
z	28	41
dA	52,600	75,000
b	15,750	14,500
x	0,1120	-0,0420

Tooth parameters

	coast	drive
alfa N	10,000	30,000
Ro max	☐	☐
Ro aP0	0,1000	0,3000
alfaKP0	11,00	30,00
hfP0	2,10	2,10
hFfP0	1,90	1,90
alfaprP0	11,00	30,00
hFaP0	2,10	2,10

Gear set parameters

beta	30,000
aW	60,000
h aP0	2,400
symmetrical tooth	☐
auto module	☐
mN	1,50000

Rotation step 1,00
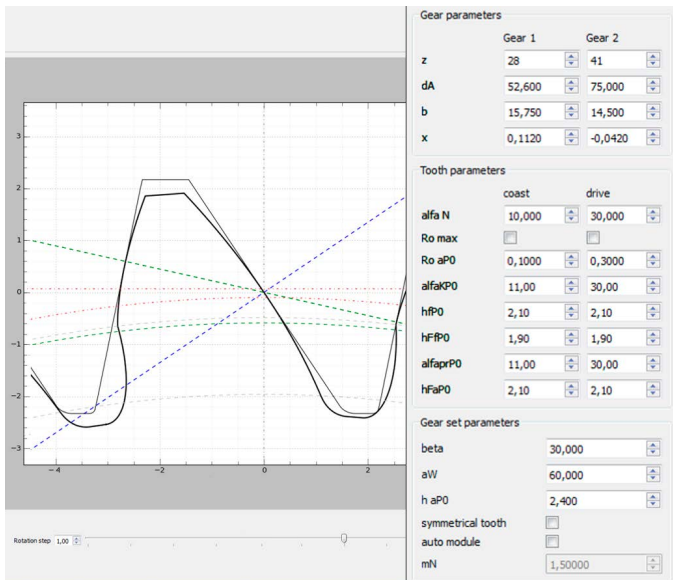
FIGURE 10: Asymmetric gear design – option "Manufacturing gear 1".
OBRÁZEK 10: Vzhled asymetrického ozubení – možnost "Výroba kola 1".

also the option of some checkboxes - for choosing of symmetric/asymmetric profile, maximum addendum rack radii at both flanks and "auto module" checkbox. This enables selection of whether the value of the normal module is calculated from other given values with no clearance (particularly the working axes distance a_w), or can be strictly determined. The second variant enables creation of the clearance between flanks. This function is very useful for preliminary design of the gearset. In the next steps, fine tuning of the profile can round this value to a more suitable one. In the upper-left corner it is possible to select "Display Options". Figure 13 gives an example of "Manufacturing gear 1". Figure 16 depicts the option "Meshing".

In addition to the gearing meshing, it is also very useful to see the situation while manufacturing. For this reason, there are more options for depiction – e.g. while manufacturing of both gears - meshing of the gear with the tool (rack) – depicted in Figure 10. The displayed variant can be chosen by clicking the button "Display Options" in the upper-left corner.
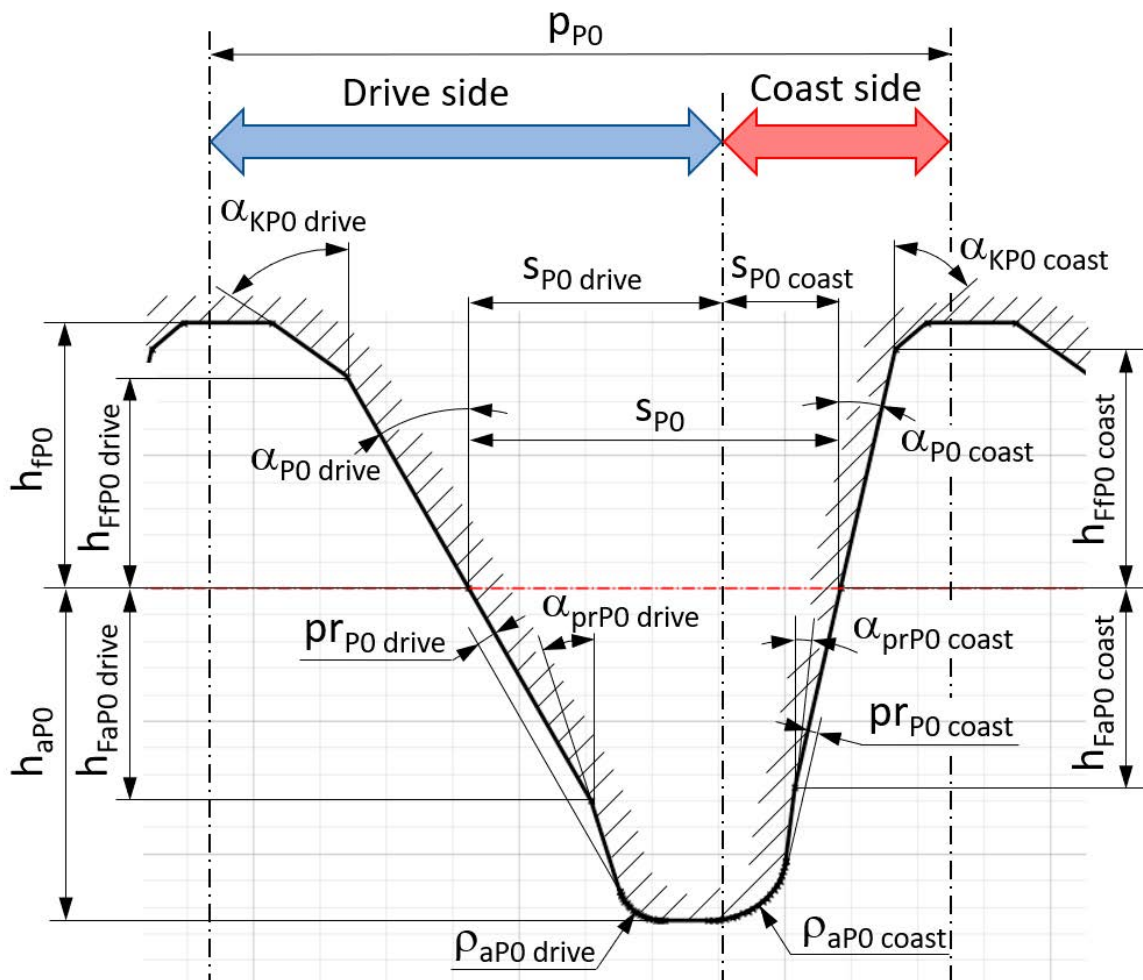
FIGURE 11: Complete appearance of manufacturing tool (rack) with asymmetric profile, tip chamfer and protuberance created by this software.
OBRÁZEK 11: Kompletní vzhled výrobního nástroje (hřeben) s asymetrickým profilem, včetně sražení na hlavě a protuberance, vytvořeno popisovaným softwarem
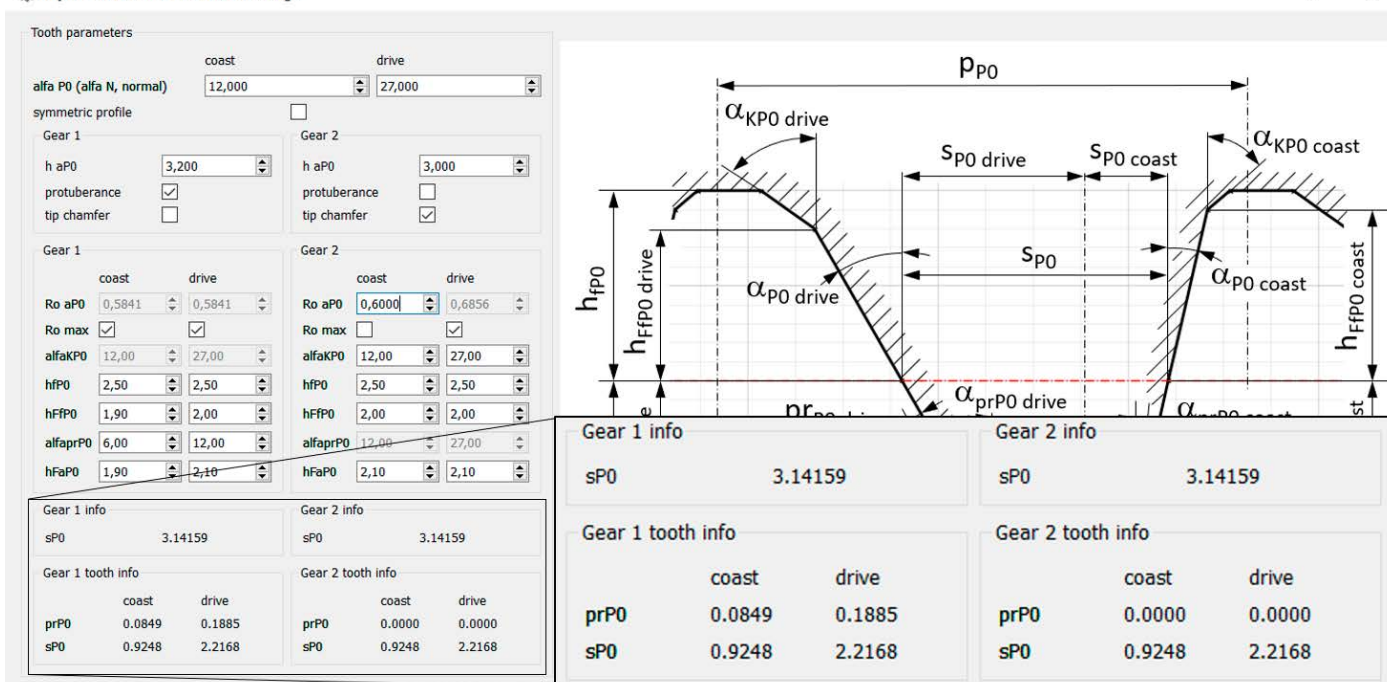
FIGURE 12: Appearance of the window for setting of a tool (rack) parameters with asymmetric profile. This window pops-up after clicking the button "Modify".
OBRÁZEK 12: Vzhled okna s nastavením parametrů nástroje (hřeben) pro asymetrický profil. Toto okno se objeví po stisknutí tlačítka "Modify"

TABLE 1: Table of input parameters of the depicted gearset in Figure 9 – for initial program version.
TABULKA 1: Tabulka vstupních parametrů soukolí, zobrazeného na Obrázku 9 – pro počáteční verzi programu.

parameter	sign	unit
Number of teeth	z_1, z_2	-
Normal module	m_n	mm
Rack profile angle - drive	α_{nD}	deg
Rack profile angle - coast	α_{nC}	deg
Helix angle	β	deg
Facewidth	b_1, b_2	mm
x – shift coefficient	x_1, x_2	-
Outer (tip) diameter	d_{a1}, d_{a2}	mm
Axes distance	a_w	mm
Addendum height of the rack (tool)	h_{aP0}	mm
Addendum radius of the rack (tool) - drive	ρ_{aP0_D}	mm
Addendum radius of the rack (tool) - coast	ρ_{aP0_C}	mm
Number of teeth to measure over	i	-
Ball diameter to measure over	D	mm

In the version depicted in Figure 10, an improvement in the tool geometry is visible in comparison with the previous version in Figure 9. It is already possible to set a tip chamfering and a protuberance. If these options are not needed, values of appropriate profile angles (α_{KP0}, α_{prP0}) are set to same value as α_n. The detailed appearance of a possible tool with tip chamfer and protuberance is depicted in Figure 11. Nevertheless, there is still only one common tool for manufacturing both gearwheels. This limitation led to an issue concerning non-equal tip – root clearance. To eliminate this issue another innovation was added to the final version. Each gearwheel has its own manufacturing tool. The only common parameters of these two tools are angles α_{P0} at both sides to assure correct mesh. All other parameters can be different e.g. addendum and dedendum heights. Furthermore, the option of tip chamfering and protuberance was maintained. In total, four separate profiles of tooth flanks are defined. All these parameters can be set in a separate pop-up window after clicking the button "Modify" depicted in Figure 13. Its appearance is depicted in Figure 12.

In Figure 13 can be seen that the checkbox "no backlash" is checked. For this reason the value of x_Σ was calculated and depicted in the tab „Gear set info" and furthermore, it is possible to set only the value of x_1 and the value of x_2 is computed automatically without a possibility to be changed.

All angles mentioned in this window (Figure 12) are parameters of the tool, so they are defined in the normal plane (e.g. rack profile angles α_{P0}). From all these parameters results the final tool geometry. Important tool parameters are depicted in the lower part, i.e. the protuberance magnitude (prP0) and tool
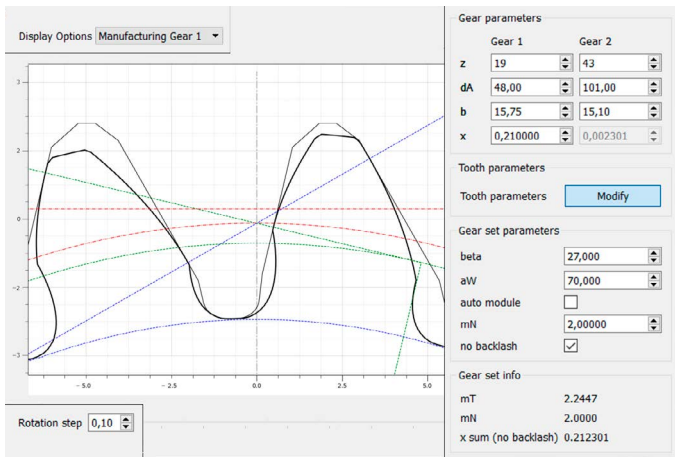
FIGURE 13: Appearance of the program including tip chamfer and protuberance – display option "Manufacturing gear 1".
OBRÁZEK 13: Vzhled programu včetně sražení na hlavně a protuberance - zobrazeno nastavení "Výroba kola 1"

thickness (s_{P0}) at the appropriate side (flank). Furthermore, total tool thickness (s_{P0}) is displayed above too. The correctness of displayed values can be checked, because for the value of normal module $m_n = 2$ mm, the value of total tool thickness s_{p0} is precisely π mm. At the gear 1 protuberance was used, at the gear 2 there is no protuberance, so the value of $prP0$ is zero at both flanks (see Figure 12).

Regarding geometry calculations, in principle the same equations are used as for symmetric gearing. For the symmetric case it is quite simple because all computed values are divided by "2"
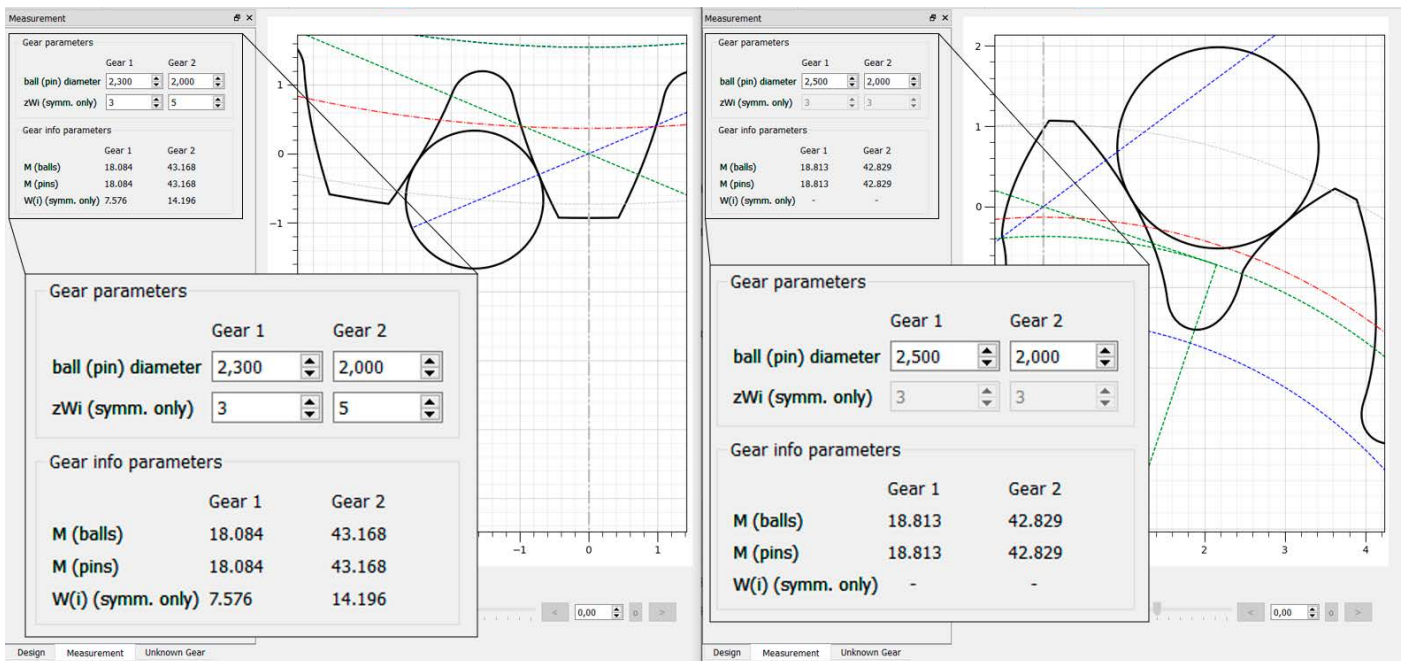
because of the symmetry. In the case of asymmetrical gearing, all these computations are leading to a system of non-linear equations which must be solved numerically by an appropriate solver. All used equations for completing the geometry calculations were found in [1], [2], [3] and [4].

These days it is possible to use it only for external, spur and helical, symmetric and asymmetric design. All necessary parameters of the gearset can be set on the left side. In the left bottom corner are three tabs: Design, Measurement and Unknown gear, see Figure 16. In the tab "Design", basic input parameters of the gearset can be entered.

Using this program it is also possible to calculate the value of the measurement over teeth (span measurement) and over balls. This can be seen in the tab "Measurement" in the bottom-left corner. In the case of symmetric teeth both these variants are possible. In the case of asymmetric gearing, only the measurement over balls is possible because there is no common tangent between opposite involute flanks. Graphical depiction of the situation with embedded ball with the diameter "D" is depicted in Figure 14 and is meaningful only for spur gearing when the depicted ball really touches both flanks. For helical gearing, the calculated value of the ball centers diameter d_g is correct, but because of the helix angle, the inserted ball does not touch the depicted transverse gear profile.

For asymmetric profile, this ball center diameter d_g can be computed from the system of two equations (27) and (28).

FIGURE 14: Appearance of the program tab "Measurement" for spur gearing with an symmetric (left) and asymmetric (right) profile. Embedded ball touches the transverse tooth profile.
OBRÁZEK 14: Vzhled záložky "Měření" pro přímé zubení se symetrickým (vlevo) a asymetrickým (vpravo) profilem. Měřicí kulička se dotýká tečného profilu zubu

$$inv\ \alpha_{gd} + inv\ \alpha_{gc} = inv\ v_d + inv\ v_c +$$

$$+ \frac{D}{d_{bd} \cdot cos\beta_{bd}} + \frac{D}{d_{bc} \cdot cos\beta_{bc}} - \frac{2 \cdot \pi}{z} \qquad (27)$$

$$\left(d_g =\right)\ \ \frac{d_{bd}}{cos\ \alpha_{gd}} = \frac{d_{bc}}{cos\ \alpha_{gc}} \qquad (28)$$

Used angles $inv\ v_d$ and $inv\ v_C$ in the formula (27) can be computed using formulas (29).

$$inv\ v_d = \frac{s_{td}}{r} + inv\ \alpha_{td}\ ,\quad inv\ v_c = \frac{s_{tc}}{r} + inv\ \alpha_{tc} \qquad (29)$$

The angular position of embedded ball related to the tooth axis is for symmetric profile given quite easily as half of the angle related to the one tooth pitch, see formula (30).

$$\varepsilon_{ball,\ symm} = \frac{2 \cdot \pi}{2 \cdot z} = \frac{\pi}{z} \qquad (30)$$

In case of asymmetric profile, this angle ε_{ball} can be derived from the Figure 15. If the diameter d_g is already known, we can focus only on the drive side, where the "touching" angle α_{tTd} is

$$\alpha_{tTd} = arctg\left(tg\ \alpha_{gd} - \frac{D}{d_{bd}}\right) \qquad (31)$$

The radius of the touching point can be computed thanks to contact angle α_{tTd} as

$$r_{Td} = \frac{r_{bd}}{cos\ \alpha_{td}} \qquad (32)$$

Tooth thickness of the drive side at this radius s_{tTd} can be subsequently computed

$$s_{tTd} = r_{Td} \cdot \left(\frac{s_{td}}{r} + inv\ \alpha_{td} - inv\ \alpha_{tTd}\right) \qquad (33)$$

To this thickness s_{tTd} relates at a radius r_{Td} an appropriate angle ε_{tTd}

$$\varepsilon_{tTd} = \frac{s_{tTd}}{r_{Td}} \qquad (34)$$

And finally, the desired angle between the tooth axis and embedded ball ε_{ball} is

$$\varepsilon_{ball} = \varepsilon_{tTd} + \alpha_{gd} - \alpha_{tTd} \qquad (35)$$

The final formula for the measurement over balls "M" is then for even number of teeth

$$M = d_g + D \qquad (36)$$

and for the gearwheels with odd number of teeth same recalculation formula as for standard symmetric profile holds true, see equation (37).

$$M = d_g \cdot cos\frac{\pi}{2 \cdot z} + D \qquad (37)$$

The tab "Unknown Gear" enables identification of unknown gear parameters using measured normal thickness at a given depth. The measured unknown gear profile can then be visually compared with the gear profile designed in the tab "Design". If both these depicted profiles match, then parameters of the unknown gear are set. This method can only be used for spur symmetric gearing and is very inaccurate.

For gearset optimizing from the perspective of qualitative properties, all necessary values are computed and depicted in the part "Gear set info" e.g. normal and tangential backlash (j_n - drive/coast), transverse contact ratio (ε_α - drive/coast), axial contact ratio (ε_β - drive/coast), total contact ratio (ε_χ - drive/coast), minimum tip thickness without chamfering (s_{na}) and minimum tip - root clearance (c_a* [-]), see Figure 16.

Coordinates of tooth flank points, which are calculated analytically, don't have the same distance between each other. To

FIGURE 15: Geometry of the measurement over balls for the asymmetric profile
OBRÁZEK 15: Geometrie měření přes kuličky, asymetrický profil

Gear set info	coast	drive
j T	0.1613	0.1439
j N	0.1283	0.1437
alfa T	13.4176	29.7632
alfa TW	14.7767	30.3531
eps Alfa	1.988	1.411
eps Beta	1.091	1.091
eps Gama	3.079	2.502

Gear info	Gear 1	Gear 2
sNa	0.838	1.062
sTa	0.966	1.205
d F	36.688	90.520
c A*	0.428	0.370

FIGURE 16: Appearance of the program including tip chamfer and protuberance – display option "Meshing". Gear 1 is depicted using interpolating spline with highlighted equidistant points.
OBRÁZEK 16: Vzhled programu, včetně sražení hlavy a protuberance - možnost nastavení "Soukolí." Kolo 1 je zobrazeno s pomocí interpolační křivky se zvýrazněnými ekvidistantními body

assure correct depicting, these calculated points are interpolated using spline curves, whose intersections are subsequently computed. This approach is applied for both intersections, i.e. for tip chamfer involute (α_{KP0}) and active involute (α_{P0}), and for active involute (α_{P0}) and tooth root fillet curve. Then these splines are defined by a given number of equidistant points. In some special cases there can occur a situation where active involute (α_{P0}) is shortened (cut) by an involute created by linear part of tool protuberance (α_{prP0}). Firstly, to find this intersection is numerically very problematic (unstable) and secondly, the magnitude of this phenomenon is very small. For these reasons, this whole part of the tooth flank is neglected in this software. These equidistant points of the tooth profile are depicted for gear 1 in Figure 16.

The final interesting property of this program can be found in a very useful function – "kinematics". It is possible to change the angular position of the gearset, so the whole "passing through the mesh" of a gear pair or the gearwheel – rack meshing, can be observed. It can be done with arrows in the bottom-right corner, see Figure 16. To be able to set a precise gear mesh position, it is possible to set the magnitude of rotational step (bottom-left corner of Figure 13) and absolute angular position of the gearset (bottom-right corner of the Figure 16). This function is very illustrative for students during lessons. Furthermore, tip root interference can be visually detected while rotating the gearset. Finally, it must also be mentioned that no commonly used deviations of all important dimensions (e.g. backlash magnitude j_n or working center distance a_w) are included in the finally designed profile. Both these gear profiles are purely theoretical. To be able to determine desired values (e.g. normal backlash j_n) including their tolerances, all input values must be set to their both tolerance extremes (maximum and minimum value in the appropriate tolerance range).

8. CONCLUSION

This contribution briefly described external involute gearing with asymmetric profile, its advantages, disadvantages and, above all, the program for its design – its previous and final appearance and functions. The formula for the sum of profile x-shift coefficient for the case of no backlash was derived. Furthermore, there was described a special property of this program regarding to displaying the gearset with a backlash due to the possibility of setting arbitrary values of the x-shift profile coefficients. All necessary basic equations were mentioned.

ACKNOWLEDGEMENTS

REFERENCES

[1] MORAVEC, Vladimír. Konstrukce strojů a zařízení II: čelní ozubená kola. Ostrava: Montanex, 2001. ISBN 80-7225-051-5.

[2] KAPELEVICH, Alexander L. Direct gear design. Boca Raton: CRC Press, Taylor & Francis Group, 2013. ISBN 978-1-4398-7618-3.

[3] NĚMČEK, Miloš. Vybrané problémy geometrie čelních ozubených kol. Ostrava: Montanex, 2003. ISBN 978-80-7225-111-7.

[4] ŠALAMOUN, Čestmír a M SUCHÝ. Čelní a šroubová soukolí s evolventním ozubením. Praha: Nakladatelství technické literatury, 1990. ISBN 978-80-03-00532-1.

EVALUATION OF PLUG-IN PARALLEL HEV TOPOLOGIES USING OPTIMAL CONTROL METHODS AND VEHICLE DYNAMICS SIMULATION

RASTISLAV TOMAN
CTU in Prague, Faculty of Mechanical Engineering; Technická 4, Praha 6, 166 07, Czech Republic; rastislav.toman@fs.cvut.cz

JOLANA HEŘMANOVÁ
CTU in Prague, Faculty of Mechanical Engineering; Technická 4, Praha 6, 166 07, Czech Republic; jolana.hermanova@fs.cvut.cz

ABSTRACT

Hybrid electric vehicle (HEV) powertrains with parallel topologies are among the frequently used layouts, because of their easy applicability on an existing conventional powertrain, by the addition of hybrid modules with mild, full, or a plug-in capability. This paper investigates three of such parallel HEV topologies: P2, P3, and P4; all in a plug-in variant, to find-out which one performs best. Apart from the topology consideration, one of the other common questions or challenges in HEV development is the ICE concept selection. To address it, the paper combines the three HEV topologies with three technologically different internal combustion engines, all with the same power outputs. Then, all the powertrain and ICE combinations are tested in homologation driving cycles and vehicle dynamics simulation test – different acceleration tests – giving a holistic methodology suitable for thorough HEV topology evaluation, identifying all possible hybridization benefits. To find the maximum CO_2 potential, it is convenient to exclude the effect of the energy management control strategy on the CO_2 result in a charge sustaining driving cycle; therefore, to use some optimal control method. For this task, the paper compares the Equivalent Consumption Minimization Strategy, that realizes a Pontryagin's minimum principle against the Dynamic Programming optimal control method, which is based on Bellman's principle of optimality. Both control methods are available as a part of GT-Suite 0D/1D/3D multi-physics CAE simulation software, that is used in our whole study.

KEYWORDS: HYBRID ELECTRIC VEHICLE, OPTIMAL CONTROL METHOD, ENERGY MANAGEMENT STRATEGY, DYNAMIC PROGRAMMING, ECMS, PONTRYAGIN'S MINIMUM PRINCIPLE, PARALLEL HYBRID POWERTRAIN TOPOLOGY, PLUG-IN HYBRID, VEHICLE DYNAMICS SIMULATION, GT-SUITE

SHRNUTÍ

Hybridní elektrická vozidla (HEV) v paralelních topologiích patří mezi běžná uspořádání zejména díky snadné aplikovatelnosti ve stávajících pohonných řetězcích přidáním hybridních modulů, a to v různých úrovních hybridizace od mild, full až po plug-in HEV. Tento článek se věnuje třem paralelním topologiím: P2, P3 a P4 v plug-in variantě s cílem jejich celkového porovnání. Kromě výběru topologie hybridního vozidla je také častou otázkou výběr konceptu spalovacího motoru vhodného pro použití v hybridním vozidle. Abychom se na tuto otázku pokusili odpovědět, porovnáváme v této práci tři topologie hybridních pohonů se třemi technicky různými spalovacími motory o stejném maximálním výkonu. Všechny varianty jsou simulovány v homologačních jízdních cyklech a dalších dynamických testech, které by měly poskytnout ucelenou metodologii pro kompletní porovnání hybridních topologií a identifikovat možné přínosy hybridizace. Při hledání maximální úspory CO_2 je vhodné omezit vliv řídící strategie na výsledné hodnoty CO_2 v „charge sustaining" módu použitím některé z optimálních metod řízení. Proto tato práce porovnává ECMS strategii, která je založena na Pontryaginově minimálním principu a metodu dynamického programování založené na Bellmanově principu optimality. Obě metody jsou dostupné jako součást 0D/1D/3D multi-fyzikálního simulačního softwaru GT-Suite, který je v celé studii využíván.

KLÍČOVÁ SLOVA: HYBRIDNÍ ELEKTRICKÉ VOZIDLO, OPTIMÁLNÍ STRATEGIE ŘÍZENÍ, ŘÍZENÍ ENERGETICKÝCH TOKŮ VE VOZIDLE, DYNAMICKÉ PROGRAMOVÁNÍ, ECMS, PONTRYAGINŮV MINIMÁLNÍ PRINCIP, TOPOLOGIE PARALELNÍHO HYBRIDNÍHO HNACÍHO ÚSTROJÍ, PLUG-IN HYBRID, SIMULACE DYNAMIKY VOZIDLA, GT-SUITE

EvaluationofPlug-inParallelHEVTopologiesUsingOptimalControlMethodsandVehicleDynamicsSimulation
RASTISLAV TOMAN, JOLANA HEŘMANOVÁ

MECCA 02 2020 PAGE 21

1. INTRODUCTION

The current mandatory fleet-wide average emission target in EU – set to 95 grams of CO_2/km starting with 2020 "phase--in" period and following full application from 2021 [1] – pushes the automotive industry into the realm of powertrain electrification. A fleet-wide electrification, either by pure electric vehicles (EV), or by hybrid electric vehicles (HEV), brings the obvious economic implications, especially the higher development and production costs.

The US and EU OEMs try to address these economic implications mainly by adopting the plug-in HEV powertrains (PHEV), combined with parallel topologies. The popularity of plug-ins from the side of OEMs is caused by two factors: first is, that the low average emission targets indirectly push for them; the second then, that a plug-in size battery allows for higher electrical power output and "fun-to-drive" factor of these vehicles. The parallel HEV topologies then give a great variety of options – usually in a form of hybrid modules applied on a conventional powertrain (ICEV) – allowing for relatively small changes in already existing powertrains, and help this way to manage development costs (especially compared to a pure EV powertrain, or more "HEV-tailored" solutions) and reduce complexity at the OEM.

However, there are many technical challenges that need to be addressed in the early development stages of any new HEV powertrain. These revolve mainly around the overall CO_2 emission reduction potential, of the chosen parallel topology, different internal combustion engine (ICE) technology, or battery size, but also – when talking about the PHEV solutions – the performance gains in dynamic tasks.

The one variable affecting the CO_2 performance of a studied HEV powertrain and its components is the energy management control strategy. It is therefore ideal to exclude its effects on the overall CO_2 results, and ensure a globally optimal solution, when performing this type of study. GT-Suite multi-physics CAE simulation software already contains two built-in optimal control strategies: Dynamic Programming algorithm (DP), and Equivalent Consumption Minimization Strategy (ECMS). DP algorithm solves the highly nonlinear HEV system's behavior, in a globally optimal manner. It is a numerical control method of solving a multi-stage decision-making optimal control problem ([2] or [3]), based on the Bellman's principle of optimality, requiring a priori information about the entire optimization horizon (in our case the entire driving cycle). Although it is not applicable for real-time control for its high computation demand, it can serve as a very good benchmarking tool, exactly according to the needs of our paper. A more computationally efficient option for the energy management strategy is the ECMS algorithm, that realizes the Pontryagin's minimum principle (PMP). Although the ECMS is also an "optimal control method", it is not intrinsically optimal as such [4], meaning it is only optimal locally in each time step, not globally during the whole driving cycle. Keeping the terminology from [4], we could further distinguish between the ECMS and PMP methods: nowadays, the term ECMS is more often used for the online causal method, whereas the PMP term is reserved for the offline non-causal application.

Some implementations of DP were used to study the optimal hybridization level in two parallel HEV topologies in [2], to instruct rule-based energy management strategies in [5, 6], to optimize the transmission's shifting strategy in [7], or to study the optimal strategy for a series-parallel Toyota Prius powertrain in [8]. Then, Zeng et al. presented an ECMS implementation as a casual suboptimal method performed online, by using several simplifying assumptions for the equivalence factor based on past and present driving in [9], or Nüesch et al. in [10] extended the Hamiltonian function with a pollutant emissions minimization. There are also some comparative studies of DP vs. PMP performance, one from Yuan et al. [11]. Finally, Zeman et al. [12] present a broad HEV topologies' CO_2 comparative study combined with modular simulation models within the GT-Suite simulation platform, using only heuristic control methods.

Our paper is divided into four main chapters, following this introductory chapter 1. Chapter 2 shows the vehicle data and parameters, together with more details on HEV topologies, and internal combustion engines (ICE). Chapter 3 then presents our benchmarking simulation methodology, different simulation models, and homologation calculations. Chapter 4 is dedicated to the results; and finally, chapter 5 presents some overall conclusions.

1.1 GOALS OF THE PAPER

The main objective of our study is to showcase and apply a full development and benchmarking methodology for HEV vehicle powertrains.

This main objective then specifies in two following goals:

- First, to present a sensitivity on a parallel HEV topology type, comparing P2, P3, and P4 variants;
- Second, to test for a synergy effect between the ICE downsizing and powertrain hybridization, comparing three ICE technologies with three different downsizing levels.

The presented methodology consists of vehicle CO_2 homologation results (using WLTP methodology), together with some dynamic tasks. These can be easily expanded with other user dynamic tasks, or driving cycles, together with future RDE cycles, or any other real-life user scenarios – if requested. All our simulation tests are carried-out on a C-class vehicle, with the same plug-in size battery, and hence pure electric drive capability (EV mode).

Evaluation of Plug-in Parallel HEV Topologies Using Optimal Control Methods and Vehicle Dynamics Simulation
RASTISLAV TOMAN, JOLANA HEŘMANOVÁ

MECCA 02 2020 PAGE 22

The additional goals of our paper are:
- To compare the two optimal control methods implemented in GT-Suite;
- To study the ECMS CO_2 sensitivity on different heuristic criteria with our HEV powertrains;
- To study the HEV powertrains' performances in some dynamic tasks (different acceleration tests, and maximum vehicle speed).

2. VEHICLE DATA AND PARAMETERS

TABLE 1: Main vehicle parameters
TABULKA 1: Hlavní parametry vozidla

Base vehicle mass	1240	[kg]
Frontal area	2.20	[m²]
Drag coefficient	0.31	[-]
Tire rolling resistance factor	0.009	[-]
Tire rolling radius	307	[mm]

We have chosen a C-class vehicle with front-wheel drive (FWD) as a baseline for all the simulations in our study. Table 1 summarizes its main vehicle parameters (base vehicle mass is without ICE). This baseline vehicle is compared to the three parallel HEV topologies (figure 1). The first two of the investigated HEV topologies – P2 and P3 – are FWD, the P4 offers the AWD (all-wheel drive) capability, although aspects such as climbing ability are not considered. P2 and P4 solutions are especially common nowadays, with P2 being probably cheaper and easier to integrate into an existing conventional powertrain (depending on the original vehicle that is hybridized). The additional masses are then in Table 2: HEV masses include high voltage battery mass of 110 kg, EM mass of 35 kg, and estimated masses for transmission adjustments, and additional clutches (K0 clutch for P2; P4 clutch).
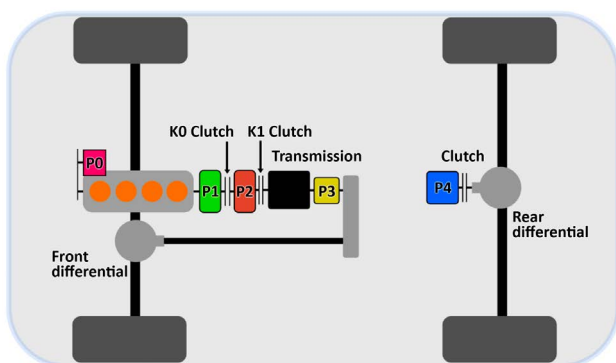
FIGURE 1: Parallel HEV topologies components' layout
OBRÁZEK 1: Uspořádání komponentů v paralelních HEV topologiích

High voltage battery is based on a Samsung SDI lithium ion prismatic battery cells with capacity of 37 Ah, and nominal voltage of 3.7 V. The battery system is then configured into 104s1p (104 cells in series, one in parallel), giving the total energy capacity of 14.8 kWh at nominal voltage of 400 V.

TABLE 2: Additional masses of ICE and HEV components
TABULKA 2: Dodatečné hmotnosti spalovacích motorů a hybridních komponentů.

2.0 NA	130	[kg]
1.5 TC	120	[kg]
1.0 TC	110	[kg]
P2 HEV	165	[kg]
P3 HEV	150	[kg]
P4 HEV	190	[kg]

The powertrain hybridization ratio (P_{ICE}/P_{EM}) is kept fixed: three ICE concepts with power output of around 135 kW are combined with the same electric motor (EM) of 54 kW (Table 3). The BSFC and efficiency maps are displayed in figure 2.

TABLE 3: ICE and EM main parameters
TABULKA 3: Hlavní parametry spalovacích motorů a elektromotoru.

	Maximum Torque [Nm]	Maximum Power [kW]	Speed Limit [RPM]	BSFC [g/kWh]	Efficiency [%]
2.0 NA	227	137	6500	224.9	-
1.5 TC	245	135	6000	237.7	-
1.0 TC	245	135	6000	238.5	-
EM	141	54	8000	-	92.9

The EM presents a classical high torque – high efficiency synchronous traction machine with permanent magnets. It is downscaled from GKN's commercial AF130 traction motor with 130 kW, keeping the same efficiency map.

Three spark ignition, direct injection ICE concepts represent different levels of ICE downsizing:
- naturally aspirated 2.0 L four cylinder (*2.0 NA*);
- turbocharged 1.5 L three cylinder (*1.5 TC*) with a BMEP of 20.5 bar;
- highly turbocharged 1.0 L three cylinder (*1.0 TC*) with a BMEP of 31.0 bar.

Evaluation of Plug-in Parallel HEV Topologies Using Optimal Control Methods and Vehicle Dynamics Simulation
RASTISLAV TOMAN, JOLANA HEŘMANOVÁ

MECCA 02 2020 PAGE 23
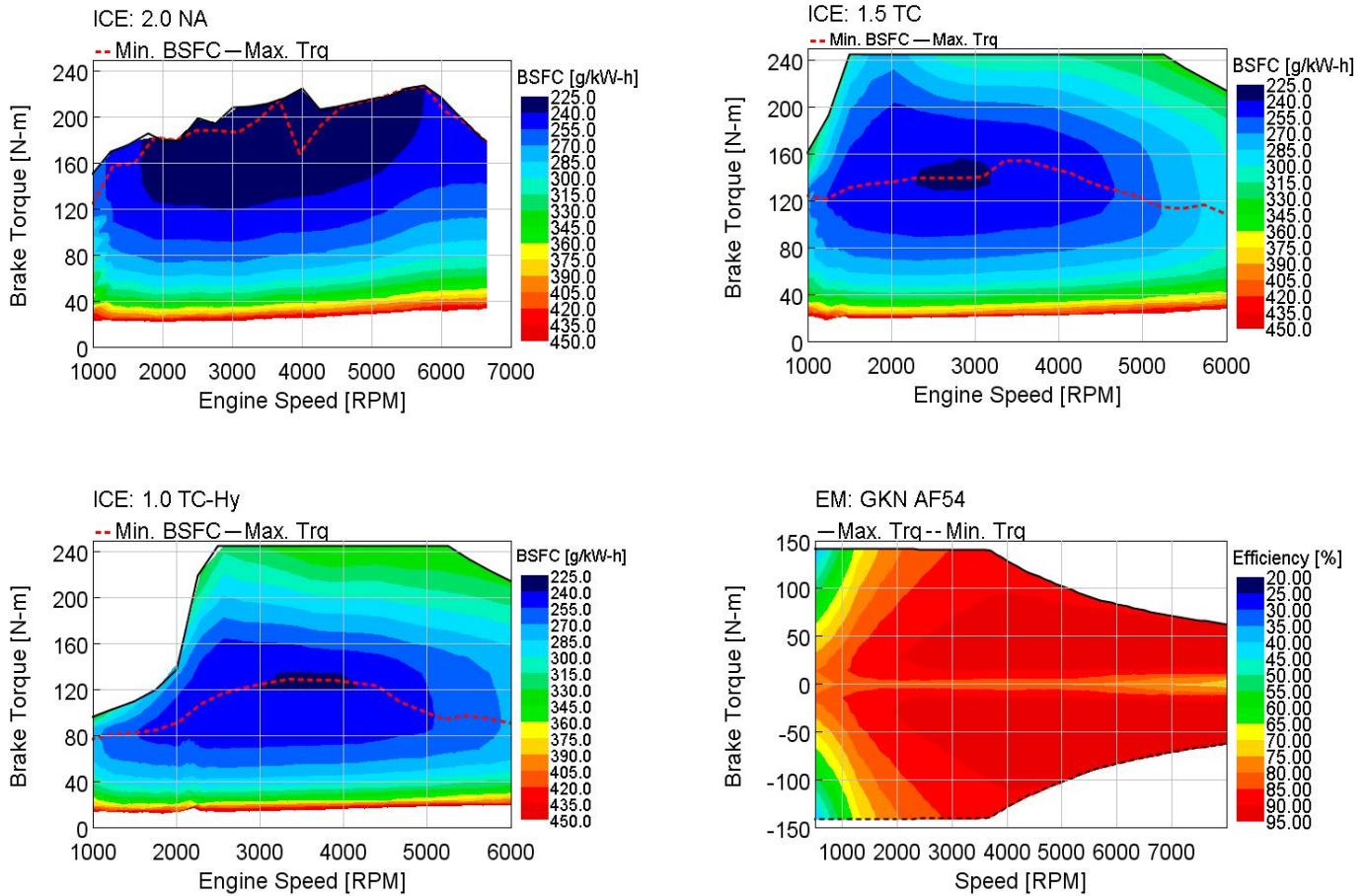
FIGURE 2: BSFC maps of ICE concepts; EM efficiency map
OBRÁZEK 2: Měrná spotřeba konceptů spalovacích motorů; mapa účinnosti elektromotoru

Turbocharged concepts use a single-stage charging system with charge-air-cooler, lowered compression ratios (compared to *2.0 NA*), together with intake and exhaust variable valve timing (VVT); the *2.0 NA* concept uses VVT only on the intake side.

The *2.0 NA* concept represents a state-of-the-art direct injection naturally aspirated engine, with the best BSFC from all concepts. A great advantage – in comparison to the turbocharged concepts – should be its relative simplicity, reliability, and therefore also cost. The *1.5 TC* concept's performance and technology represent a standard in current downsizing era. The *1.0 TC* should be the best from the packaging and mass viewpoint. However, this is offset by higher price, and poorer low-end-torque performance.

All three ICE concepts are matched to a distinct six-speed transmission with progressive and sporty gear ratios (figure 3). The transmissions' efficiencies are taken from a similar production transmission, the other driveline efficiencies are kept constant. P4 variant adds a single-speed transmission, again with constant efficiency, and total gear ratio of 6.2 (transmission

gear ratio of 2.48 and differential gear ratio of 2.5), that allows for the EM use below 150 km/h, then it is de-clutched.

3. SIMULATION METHODOLOGY

There are two basic vehicle simulation methods in GT-Suite: a kinematic method, and a dynamic method. Our simulation methodology fully exploits these two different modelling options, together with the modularity of GT-Suite simulation software package.

The first one – backward kinematic – calculates the ICE/EM operating point from the imposed vehicle speed, and from the vehicle external loads (optionally imposing ICE/EM speed and load, then called a forward kinematic method).

The second method – dynamic – performs the physical sequence of actions as in the real-life vehicle with a driver: driver operates the accelerator and brake pedals, and shifts gears; his commands are then interpreted in an ECU model, and sent to the plant models (ICE, EM, etc.), the same way as in a real vehicle, resulting in vehicle acceleration.

EvaluationofPlug-inParallelHEVTopologiesUsingOptimalControlMethodsandVehicleDynamicsSimulation
RASTISLAV TOMAN, JOLANA HEŘMANOVÁ

MECCA 02 2020 PAGE 24

1.0 TC Transmission

60 [km/h] 91 [km/h] 129 [km/h] 174 [km/h] 221 [km/h]

6000 [RPM]

5016 [RPM]
4732 [RPM]
4464 [RPM]
4212 [RPM]
3973 [RPM]

Gear Ratio 1 = 3.420
Gear Ratio 2 = 2.265
Gear Ratio 3 = 1.590
Gear Ratio 4 = 1.183
Gear Ratio 5 = 0.933
Gear Ratio 6 = 0.780
FD Ratio = 3.400

1.5 TC Transmission

60 [km/h] 91 [km/h] 129 [km/h] 173 [km/h] 219 [km/h]

6000 [RPM]

5022 [RPM]
4738 [RPM]
4470 [RPM]
4217 [RPM]
3978 [RPM]

Gear Ratio 1 = 3.530
Gear Ratio 2 = 2.340
Gear Ratio 3 = 1.645
Gear Ratio 4 = 1.225
Gear Ratio 5 = 0.968
Gear Ratio 6 = 0.810
FD Ratio = 3.300

2.0 NA Transmission

60 [km/h] 90 [km/h] 129 [km/h] 173 [km/h] 220 [km/h]

6500 [RPM]

5430 [RPM]
5123 [RPM]
4833 [RPM]
4559 [RPM]
4301 [RPM]

Gear Ratio 1 = 3.520
Gear Ratio 2 = 2.329
Gear Ratio 3 = 1.634
Gear Ratio 4 = 1.215
Gear Ratio 5 = 0.958
Gear Ratio 6 = 0.800
FD Ratio = 3.600

FIGURE 3: Transmission layouts for all three ICE concepts
OBRÁZEK 3: Pilové diagramy tří použitých převodovek

The next chapters from 3.1. to 3.5. give a comprehensive look on the use of the two vehicle simulation methods in our studies: 3.1. shows how we work with these different simulation models; then we discuss the two optimal control methods (in 3.2. and 3.3.) with some heuristic criteria (in 3.4.); and 3.5. finally shows the different simulation test, that serve either for benchmark studies, or for vehicle homologation results.

3.1. SIMULATION MODELS

There are two models for each HEV powertrain topology: a dynamic model (DYN), and a kinematic model (KIN). Both are built using interchangeable modules or sub-systems (e.g. ICE model, EM model, HV-Battery model etc.) for each simulation method, with the same database containing the vehicle data and parameters from chapter 2. This combined approach of using modular models in combination with parameter database aids the general use and simulation work, together with simple possible replacement of some sub-system with a new one, that for instance accounts for more detailed physical behavior, or control logic. These changes can be then done easily and quickly for each HEV powertrain model.

KIN models are used for the ICEV CO_2 results simulation and since the optimal control methods – that will be discussed in next chapters – are coupled with the kinematic method, also the "Charge sustaining" (CS) CO_2 results. DYN models are then used for the E-range estimation and all other vehicle dynamics studies.

Driveline model in GT-Suite is built by the combination with 1D inertias with either rigid or compliant connections. The vehicle data in our simulation models (KIN and DYN) are then mostly map based.

High voltage battery is simulated as a resistive electrical-equivalent model with separate open-circuit voltage, and internal resistance maps for charge and discharge.

Then, combustion engines are simulated through map-based models with fuel consumption maps, and torque limits dependent on rotational speed. This map-based approach for the ICE simulation does not capture well the dynamic effects in transient behavior, which is especially apparent for the turbocharged ICE concepts at vehicle dynamics test. On the other hand, the map-based approach is very simple and giving fast simulation times, and its accuracy in the driving cycle simulation depends on ICEs relative power to the total vehicle loads (smaller ICE leads to more demanding transient behavior). The problem with ICE transients can be mitigated with additional torque rise limit maps (in [Nm/s]), or by more detailed physical ICE sub-system using either full 1D or simplified 1D fast-running model. However, these are not used in our study.

EvaluationofPlug-inParallelHEVTopologiesUsingOptimalControlMethodsandVehicleDynamicsSimulation
RASTISLAV TOMAN, JOLANA HEŘMANOVÁ

MECCA 02 2020 PAGE 25

The EM model is also map-based with an efficiency map, and torque limits dependent on the rotational speed. Thanks to the very fast EMs transient response, the map-based approach is accurate enough.

Finally, also the transmission models are map-based (together with other gear ratios), with efficiencies that are taken from a similar production manual transmission, and maps dependent on input torque, rotational speed, and engaged gear.

3.2. DYNAMIC PROGRAMMING CONTROL METHOD IN GT-SUITE

Bellman's principle of optimality used in the DP control method states [13]: *"An optimal policy has the property that whatever the initial state and initial decision are, the remaining decisions must constitute an optimal policy with regard to the state resulting from the first decision. A complex multistage optimal problem can be divided into a series of single-stage optimal problem. Each single-stage optimal problem is solved by optimal solutions, and cost function is minimized according to a sequence of decisions for each step."*

DP algorithm implementation within GT-Suite is described in more detail in [3], therefore, we will reproduce only some of the most important concepts here.

The DP cost function J is defined by the equation 1, where:

- $g_N(x_N)$ represents the final cost, and additional Terminal State Penalty $T_N(x_N)$, that partially constrains the final state;
- Function $L_k(x_k, u_k(x_k))$ represents the cost of applying control $\mu_k(x_k)$ at x_k, according to the control problem's Hamiltonian function;

$$J_\pi(x_0) = g_N(x_N) + T_N(x_N) + \sum_{k=0}^{N=1} L_k(x_k, u_k(x_k)) + p_k(x_k) \quad (1)$$

T_N is then defined in equation 2, with its Terminal State Penalty Weight γ, and Terminal State Penalty Exponent β. Penalty function $p_k(x_k)$ enforces the state constraints for $k = 0, 1, \dots, N-1$. Equation 3 gives the definition of $p_k(x_k)$, with Penalty Function Weight λ, and Penalty Function Exponent α.

Battery SOC related units here are the SOC limits SOC_{max} and SOC_{min}, Target Battery SOC SOC_{target}, and the discretized SOC points SOC_{grid}, that is used only in the equation 2.

$$T_N = \gamma(SOC_{grid} - SOC_{target})^\beta \quad (2)$$

$$p(SOC) = \lambda \left(\frac{SOC(t) - SOC_{target}}{\frac{(SOC_{max} - SOC_{min})}{2}} \right)^\alpha \quad (3)$$

The optimal policy minimizes $J_\pi(x_0)$ for all admissible policies – meaning control inputs (e.g. powertrain mode, electrical motor torque, transmission gear etc.), where π is the set of all of them (equation 4).

$$J^*(x_0) = \min_{x \in \pi} J_\pi(x_0) \quad (4)$$

Based on the principle of optimality, DP evaluates the optimal cost-to-go function $J_\pi(x^i)$ – or optimal control trajectory – at every node in discretized grid points (x_k^i is one of the state variables, at a node with time index k and state index i), with SOC being the state variable (DP implementation in GT-Suite version v2020 uses only one state variable – SOC). DP then proceeds backward in time, with equation 5 yielding the end cost calculation, and equation 6 the cost calculation for steps $k = 0, 1, \dots, N-1$.

$$J_N(x^i) = g_N(x^i) + T_N(x^i) \quad (5)$$

$$J_k(x^i) = \min_{u_k \in U_k} \left\{ L_k(x^i, u_k) + p_k(x_k) \dots + J_{k+1}(f_k(x^i, u_k)) \right\} \quad (6)$$

The right-hand side of equation 6 is minimized at each state-time node, for each x_k^i leading to the optimal control policy. However, $J_{k+1}(x)$ is only evaluated for discretized points; output function $f_k(x^i, u_k)$ must be interpolated, since the state output is continuous in the state space, and so generally does not coincide with the state grid nodes. This introduces numerical errors and bounds the solution's accuracy to the discretization of the state space, and control inputs. If the discretization resolution increases, also the DP's accuracy increases. Though, also the computation load is higher. Outputs from equations 5 and 6 create the optimal control map, from which the algorithm derives the optimal control trajectory.

A challenge for each new DP simulation problem is to understand the results' sensitivity on state variable resolution and limits (min/max values); sensitivities on four penalty parameters from equations 2 (β, γ) and 3 (α, λ); and sensitivity on control variables' discretization. This process can be very time consuming, but necessary.

3.3. ECMS CONTROL METHOD IN GT-SUITE

The equivalent consumption in ECMS refers in its basic form in equation 7, to converting the battery power P_b to an equivalent fuel power by using a non-dimensional equivalence factor s, and adding it to an actual fuel power P_f [4].

$$H(t, s, u) = P_f(t, u) + s(t) \cdot P_b(t, u) \quad (7)$$

This equivalence factor s depends on the driving cycle, and on battery initial/final conditions; it represents the cost of recharging

the battery power in future (by regenerative braking or ICE charging). Therefore, to set the equivalence factor accurately, the future conditions (e.g. the driving cycle) need to be known beforehand (either for the online or offline applications).

ECMS algorithm implementation in GT-Suite calculates the equivalent fuel consumption using the equation 8, combining the equivalence factor s, with a penalty function p. The equivalence factor s can generally vary during the driving cycle, however in this implementation it is used as a constant.

The penalty function p (equation 9) helps to keep the SOC within the certain limits and thus reach the final SOC state at the end of the simulated driving cycle, where the penalty function's exponent α changes it's "aggressiveness" with SOC value deviating from SOC_{target}.

The user then controls the ECMS by varying these two parameters: equivalence factor s, and the penalty function exponent α (Note: the penalty function exponent α is not related to the one used in DP and can generally have different integer values). To simulate a "charge-sustaining" (CS) cycle, the "optimal" value of the s factor must be found for the chosen hybrid powertrain and its initial/final conditions.

$$\dot{m}_{eqv}(t) = \dot{m}_f(t) + \frac{s}{Q_{LHV}} \cdot P_{batt}(t) \cdot p(SOC) \qquad (8)$$

$$p(SOC) = 1 - \left(\frac{SOC(t) - SOC_{target}}{\frac{(SOC_{max} - SOC_{min})}{2}} \right)^{\alpha} \qquad (9)$$

We could say, that based on the terminology mentioned in the introductory chapter from [4], this GT-Suite's implementation could be called a PMP method, since it works offline, and in combination with iterative approach to find the equivalence factor s. Also, the nature of this implementation – numerical minimization of the equivalent fuel consumption in each time step – should lead to an "aggressive" behavior and results close to DP control method – Yuan et al. [11] presented a difference only of 0.4% between the two methods.

3.4. ADDITIONAL HEURISTIC CONDITIONS FOR OPTIMAL CONTROL METHODS

When using either one of the optimal control algorithms above, it is suitable to have some additional options to "guide" the algorithm apart from the basic limits, such as battery or EM power limits etc. These can represent real-life scenarios and limits, that cannot be imposed by the simple control limits: e.g. forced ICE starts to account for heating of the catalytic converter, limiting conditions on the use of EV mode to ensure more predictable powertrain mode switching behavior, or imposing the limit conditions on maximum allowable

gear when optimizing the gear shifting strategy. This way the user can get some idea of an impact of these criteria or conditions on the global FC (fuel consumption) optima.

In the case of ECMS, this can further improve its results – and in some cases ensure method's convergence to CS result, which is not guaranteed (as will be shown in a chapter 4.5). When we have a look on the WLTC and CS simulation, the local ECMS's optimality leads to an almost continual battery charge roughly in the first half of the cycle, followed by discharge during the second half (figure 4, blue line). This results in sub-optimal fuel consumption for the CS cycle and PHEV powertrain from the global point of view.
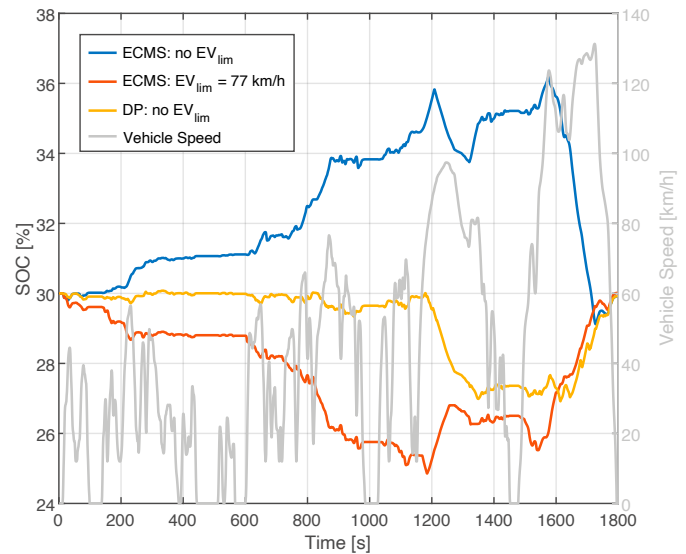

FIGURE 4: SOC comparison of DP vs. ECMS with EV_{lim} heuristic parameter turned on/off in CS WLTC
OBRÁZEK 4: Porovnání průběhů SOC algoritmů DP a ECMS s heuristickým parametrem EV_{lim} zapnutým/vypnutým v „charge sustaining" módu jízdního cyklu WLTC

This specific problem can be mitigated by the additional heuristic criteria, that limits the maximum vehicle speed, when the electric motor can act as a "primary mover" (EV_{lim}). Above this limit, the electric motor can only fulfill the load point shifting function. Similar methods are listed in [4]. The addition of EV_{lim} changes the "charge sustaining equivalence factor s", and also affects the overall powertrain behavior: the battery discharges in the first phases of the cycle, and charges in the later phases, improving the overall fuel consumption (figure 4, green line). Red line in figure 4 represents the SOC obtained with the DP algorithm.

3.5. SIMULATION TYPES AND CO$_2$ HOMOLOGATION CALCULATIONS

Since one of the goals of this paper is to give a comprehensive benchmarking study of the three HEV topologies combined with three representatives of ICE downsizing level, here we

Evaluation of Plug-in Parallel HEV Topologies Using Optimal Control Methods and Vehicle Dynamics Simulation
RASTISLAV TOMAN, JOLANA HEŘMANOVÁ

MECCA   02 2020   PAGE 27

enumerate all simulation types and calculations, whose results will be presented in the next result chapter:

- First, there are two simulation tasks, that use KIN models: ICEV CO_2 and CS CO_2 (the latter combined with the two optimal control strategies);
- Second, the All Electric Range (AER) simulations using DYN models;
- Third, homologation CO_2 can be calculated from AER and CS CO_2 results, using the utility factor (UF) according to the WLTP homologation procedure – brief description follows;
- Fourth and final are the vehicle dynamics simulations using DYN models.

CO_2 homologation procedure of hybrid vehicles (OVC-HEVs – Off-Vehicle Charging Hybrid Electric Vehicles) according to WLTP includes mainly CS, "Charge Depleting" (CD), and AER test [14]. The final combined WLTP fuel consumption (FC_{WLTP}) is calculated from CS and CD consumptions, and UF corresponding to the AER, according the equation 10.

$$FC_{WLTP} = \sum_{j=1}^{k} \left(UF_j \times FC_{CD,j} \right) + \left(1 - \sum_{j=1}^{k} UF_j \right) \times FC_{CS} \quad (10)$$

The fractional utility factor UF_j is determined by the equation 11 for a distance d_j driven at the jth period of the WLTC: C_i is a set of coefficients determined by the WLTP standard, and d_n represents a normalized distance.

$$UF_j(d_j) = 1 - \exp\left\{ -\left(\sum_{i=1}^{k} C_i \times \left(\frac{d_j}{d_n} \right)^i \right) \right\} - \sum_{l=1}^{j-1} UF_l \quad (11)$$

The All Electric Range represents a distance driven from fully charged battery, until the WLTC phase, when the engine first starts.

4. SIMULATION RESULTS

The WLTP requires a CS, and AER tests for CO_2 or fuel consumption evaluation. Since the analyzed powertrains are all PHEV type, the CS driving cycle initial and target SOC values are set to 30%, which would correspond to a usual PHEV battery use: when the battery is charged, the vehicle uses mostly EV mode; then if the SOC level is low (usually around 20-30% SOC) it switches to HEV mode.

During the entire CS test all three topologies can use the ICE load-point-shifting (LPS) in HEV mode (in case of P4 it is "through-the-road"), together with EV mode. The optimal use of EV to HEV mode switching, and LPS is determined by the DP or ECMS control algorithms, switching the ICE off in the EV mode.

The AER tests start at SOC of 96%, the AER test stops then at 35%. Similarly, the vehicle dynamics tests start with full battery (HEV and EV tests), disregarding any derating behavior of the electrical components.

Regarding the gear shifting strategy, all the sets of results, except for 4.3, use shifting strategy generated by the WLTP. The sensitivity in 4.3 compares the WLTP strategy with the "DP-optimized" shifting, only for the P2 topology.

The combination of CO_2 homologation simulations and vehicle dynamics tasks presents a full development and benchmarking methodology for HEV powertrains comparison. The results show the sensitivities on a topology type and a synergy effect between the ICE downsizing and powertrain hybridization. The vehicle dynamic tests results further show the importance of holistic approach to the optimization of these powertrains.

4.1. ICEV SENSITIVITY ON ICE TECHNOLOGY

This first ICEV powertrain sensitivity on different ICE concepts (Table 4) reveals an anticipated fact, that the downsized engines provide better fuel economy in homologation driving cycles. Higher ICE downsizing levels achieve lower fuel consumption and CO_2 production.

TABLE 4: Fuel consumption and CO_2 sensitivity on different ICE concepts
TABULKA 4: Spotřeba paliva a produkce CO_2 pro různé koncepty spalovacích motorů

ICE	FC [L/100km]	CO_2 [g/km]
2.0 NA	6.115	139.42
1.5 TC	5.777	131.72
1.0 TC	5.251	119.72

4.2. OVERALL FC/CO_2 RESULTS (HEV TOPOLOGIES VS. ICE CONCEPTS)

Table 5 shows the overall results of all three PHEV topologies, combined with the three ICE concepts: CS mode and combined values, together with AER, UF, and ΔCO_2 potential compared to respective ICEV concepts. The CS mode results were simulated using DP control method, with the SOC resolution (SOC_{grid}) of 1% (101 SOC levels), with EV_{lim} parameter turned off.

First main observation is that the P4 topology has the biggest overall homologation CO_2 potential (ΔCO_2 in the last column in table 5), followed by P2, and P3 topologies. The same applies for the AER values, that dictate the UF then used for the combined homologation FC/CO_2 calculation (equations 10 and 11, with CD mode gCO_2/km equal to zero).

Considering that the P3 and P4 topologies work in a very similar way, the AER potential and subsequent combined FC results are

EvaluationofPlug-inParallelHEVTopologiesUsingOptimalControlMethodsandVehicleDynamicsSimulation
RASTISLAV TOMAN, JOLANA HEŘMANOVÁ

MECCA 02 2020 PAGE 28

	ICE	CS mode FC [L/100km]	CS mode CO_2 [g/km]	AER [km]	UF [-]	Combined FC [L/100km]	Combined CO_2 [g/km]	Combined ΔCO_2 [g/km]
	2.0 NA	4.446	101.37	62.5	0.777	0.989	22.56	-116.86
P2W	1.5 TC	4.618	105.29	62.2	0.777	1.028	23.43	-108.28
	1.0 TC	4.438	101.19	62.3	0.777	0.988	22.52	-97.20
	2.0 NA	4.273	97.42	56.1	0.753	1.058	24.11	-115.31
P3	1.5 TC	4.506	102.74	53.6	0.734	1.198	27.32	-104.40
	1.0 TC	4.378	99.82	55.0	0.753	1.084	24.70	-95.02
	2.0 NA	4.213	96.06	66.4	0.777	0.938	21.38	-118.05
P4	1.5 TC	4.364	99.50	66.7	0.777	0.971	22.14	-109.57
	1.0 TC	4.293	97.88	66.9	0.777	0.955	21.78	-97.94

much better for the P4. The difference comes mainly from the much more favorable total gear ratio for the P4, together with better efficiencies in EV mode. The comparison of EM operating points in figure 5 indicates, that the EM in P3 topologies spends a lot of time in low speed – high torque regions; the P4 gear ratio on the other hand allows for generally higher EM operating speeds with better overall efficiencies.

A natural expectation for the P2 topology is, that it would use the ability to shift gears also in EV mode to offset the transmission efficiency disadvantage (compared for instance to P3 or P4). However, for the case of overall results, the gear shifting strategy comes from WLTP – generated based on ICE performance, not EMs – which proves to be problematic. It is once again in full display in figure 5 with EM operating points,
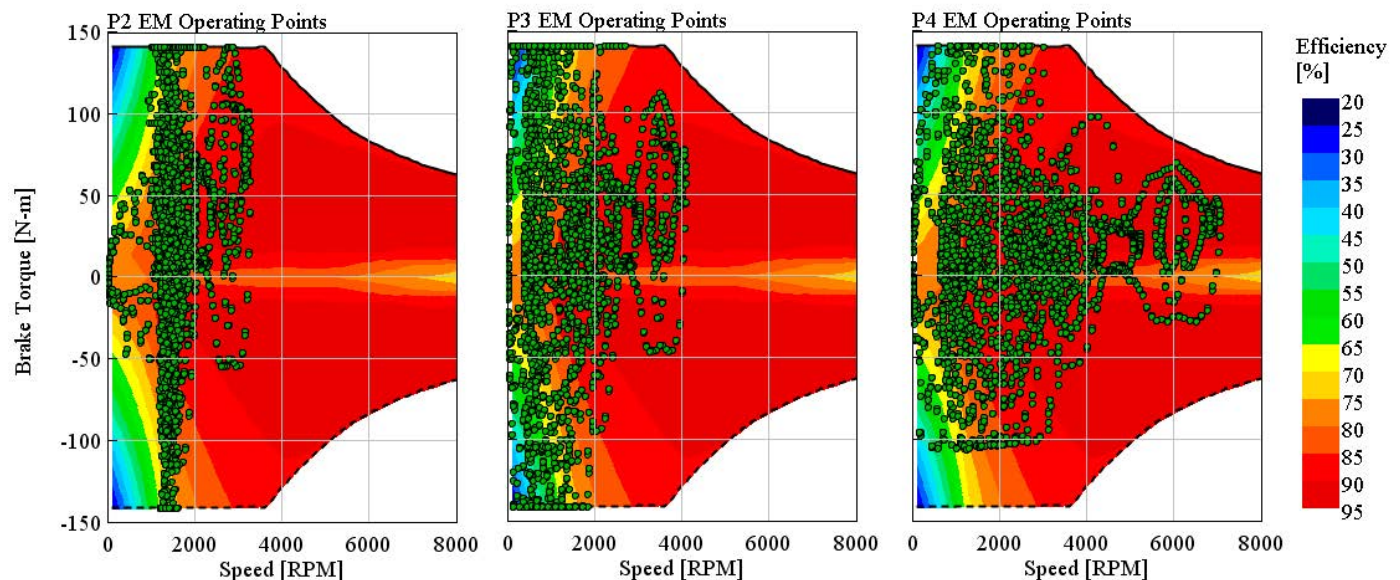
FIGURE 5: EM operating points in WLTC, driven in EV mode
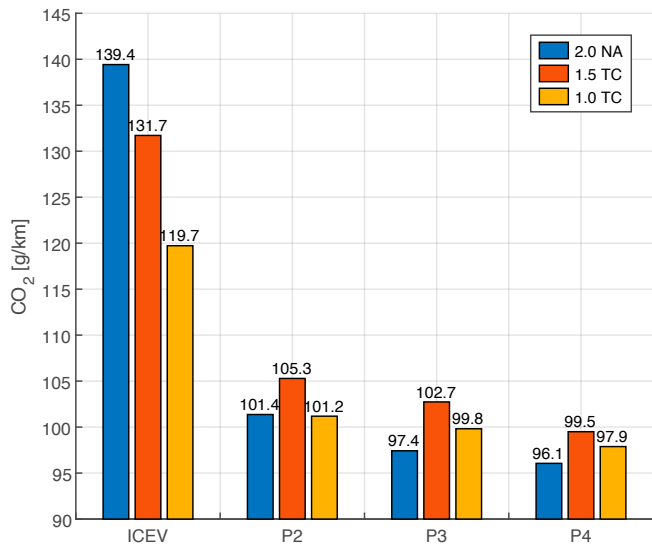**OBRÁZEK 5:** Pracovní body elektromotoru v jízdním cyklu WLTC, v elektrickém módu

EvaluationofPlug-inParallelHEVTopologiesUsingOptimalControlMethodsandVehicleDynamicsSimulation
RASTISLAV TOMAN, JOLANA HEŘMANOVÁ

MECCA 02 2020 PAGE 29

FIGURE 6: Overall CS mode CO$_2$ results (topologies vs. ICE concepts)
OBRÁZEK 6: Celkové výsledky produkce CO$_2$ v „charge sustaining" módu (topologie HEV vs. koncepty spalovacích motorů)

FIGURE 7: P2 topology CO$_2$ sensitivity on gear shifting
OBRÁZEK 7: CO$_2$ citlivost topologie P2 na průběh řazení

where the EM operating points for P2 are "compressed" to the low speed regions with lower efficiencies.

Figure 6 depicts the CS mode CO$_2$ values only, and gives us another interesting observation, that the best CS mode results are achieved with *2.0 NA* concept and not with the turbocharged concepts: there is no synergy effect between the powertrain hybridization and ICE downsizing. The explanation lays in the BSFC maps: *2.0 NA* best value is 12.8/13.7 g/kWh better compared to *1.5 TC* and *1.0 TC* respectively. CO$_2$ value for *1.0 TC* in ICEV powertrain is already very good, thus it's hybridization CS mode potential in all PHEV topologies is the smallest. However, for *1.5 TC* versus *1.0 TC* comparison the downsizing effect is lowered by the effect of powertrain hybridization.

From the vehicle homologation perspective, these CS mode sensitivities do not play any role. The only important result is the combined CO$_2$ values from the table 5, where the WLTP calculation clearly prefers the AER before the CS mode. However, the CS mode results could be interesting from the point of view of the OEMs: cheaper, higher-displacement ICEs, hybridized in a clever way can bring some economic benefits.

4.3. P2 SENSITIVITY ON GEAR SHIFTING

The overall results from the above chapter showed P2 fuel consumption using WLTP generated gear shifting points. Further gear shifting optimization using DP algorithm for the P2 topology in CS mode shows another CO$_2$ potential ("DP-optimized" in and figure 7) in comparison to the WLTP shifting strategy.

The *1.5 TC* and *2.0 NA* concept achieve a very similar additional CS mode CO$_2$ improvement (both at ~10 gCO$_2$/km), and the *1.0 TC* only ~5 gCO$_2$/km.
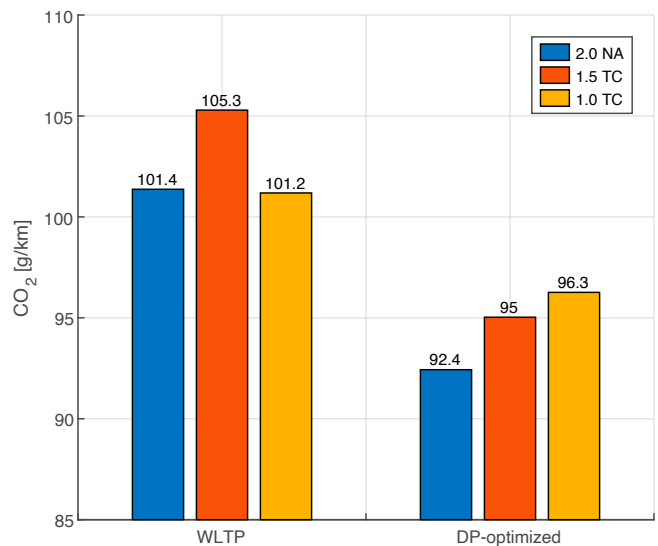
We did not calculate the further CO$_2$ potential from the homologation perspective, because this requires also the AER simulation with optimized gear shifting strategy. However, the CS mode improvement indicates, that the AER results will also be improved, leading to even lower homologation CO$_2$ values. Concluding this sensitivity, it is important to once again stress, that *2.0 NA* concept still proves having the highest hybridization potential.

4.4. DP VS. ECMS CONTROL STRATEGY SENSITIVITY

This next sensitivity compares ECMS and DP algorithms' performance. Figure 8 shows three of the nine total combinations
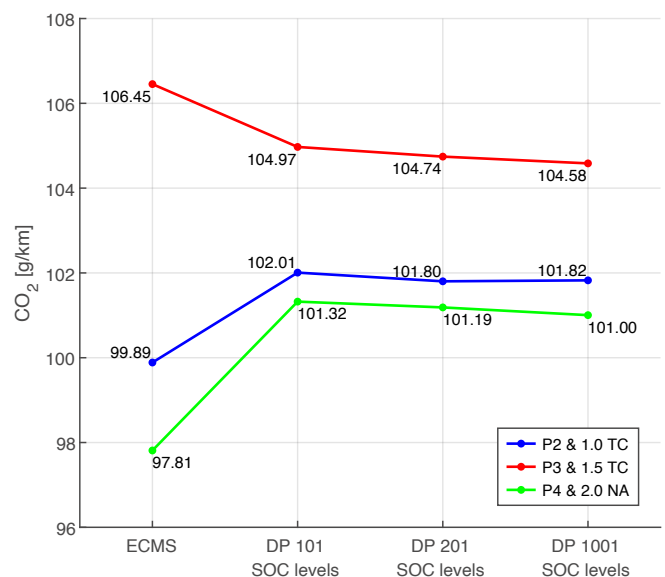

FIGURE 8: Control strategy CO$_2$ sensitivity in CS mode
OBRÁZEK 8: CO$_2$ citlivost řídících strategií v "charge sustaining" módu

of HEV topology and ICE concept. All the results use the same EV_{lim} parameter of 77 km/h. For the ECMS results, we had to calibrate the equivalence factor s for each of the simulations – to reach the CS cycle; for the DP simulations we have tried different SOC resolutions, starting with 1% of the SOC span (defined by the SOC_{max} and SOC_{min} values), that divides the SOC span to 101 SOC levels. The 0.5% resolution uses 201 levels, and 0.1% 1001 levels. Higher number of SOC level leads to results closer to global optimum, but also the simulation times are longer: 0.1% resolution leads to approximately 10-times longer simulation than 1%.

However, a look on figure 8 reveals, that the GT-Suite's ECMS implementation performs better than DP implementation for two of the three topologies (results are consistent for all ICE concepts). The only case when the DP is closer to a global optimum are the P3 topology results. Differences of FC/CO_2 are in favor of ECMS for the P2 (~2%), and P4 (~4%), and in favor of the DP (~1.5%) for the case of P3 topology.

It is also important to note, that the procedure of finding the CS equivalence factor s requires an iterative process – usually 20-40 simulations. It takes approximately the same simulation time to reach the CS results with ECMS, as to simulate one DP run with 1% SOC resolution.

The first reason for the rather unexpected result for the P2 and P4 topologies can be the way how the ECMS and DP use their penalty functions: it is possible, that using the same formulation of penalty functions, or not using any at all, could
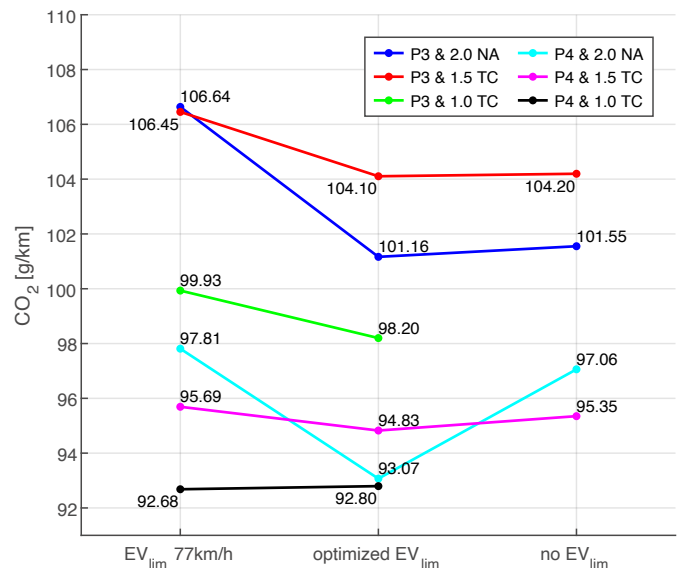

FIGURE 9: ECMS control strategy CO_2 sensitivity on heuristic parameter EV_{lim} in CS mode
OBRÁZEK 9: CO_2 citlivost řídící strategie ECMS na heuristický parametr EV_{lim} v „charge sustaining" módu

resolve the difference. The second possible reason is the different sensitivities of both methods on control variables, that were set-up the same way in our simulations.

However, from the user point of view, the simulations with DP algorithm may take more time, and not always reach the global optima "as advertised", but they may be more comfortable to work with, since they do not require the iterative process of

TABLE 6: Acceleration results for *2.0 NA* concept and all HEV topologies
TABULKA 6: Akcelerace pro koncept spalovacího motoru *2.0 NA* a všechny HEV topologie

Mode	Topology	0-100 km/h [s]	60-80 km/h [s]		60-100 km/h [s]		80-120 km/h [s]	
			Gear 5	Gear 6	Gear 5	Gear 6	Gear 5	Gear 6
HEV	P2	5.1	3.1	3.7	5.8	7.2	5.8	7.4
	P3	6.3	3.0	3.2	5.6	6.3	5.6	6.5
	P4	5.8	2.4	2.5	4.8	5.3	5.4	6.1
ICEV	P2	8.2	5.7	7.0	10.9	14.1	10.7	14.5
	P3	8.1	5.7	7.0	10.9	14.1	10.7	14.5
	P4	8.3	5.8	7.1	11.1	14.4	10.9	14.8
EV	P2	15.8	7.1	9.3	15.3	19.4	16.9	22.2
	P3	32.2	6.9	6.8	14.0	14.0	15.4	15.4
	P4	20.3	4.1	4.1	9.6	9.6	13.7	13.7

EvaluationofPlug-inParallelHEVTopologiesUsingOptimalControlMethodsandVehicleDynamicsSimulation
RASTISLAV TOMAN, JOLANA HEŘMANOVÁ

MECCA 02 2020 PAGE 31

equivalence factor s calibrations. The crucial fact is, that the results for both the ECMS and DP GT-Suite implementations are qualitatively the same (general behavior is the same with all ICE concepts and HEV topologies), although quantitatively there are some differences.

4.5. ECMS SENSITIVITY ON MAXIMUM VEHICLE SPEED IN EV MODE

The last set of CS mode simulations is the ECMS control method sensitivity on the EV_{lim} parameter. Similarly, as for the penultimate sensitivity in chapter 4.4, we show only some of the results. The optimized EV_{lim} values generally achieve the best CO_2 results (figure 9). But, the sensitivity of all ICE concept and HEV topology combinations in CS mode vary:

- P4 topology with $1.0\ TC$ concept, and all the P2 combinations are not able to reach the CS mode in simulations with EV_{lim} parameter turned off (explanation in chapter 3.4);
- $2.0\ NA$ concept – for all topologies – achieves the best results using EV_{lim} above 100 km/h;
- P3 topology also achieves the best results using EV_{lim} above 100 km/h – for all ICE concepts;
- $1.0\ TC$ concept uses relatively low EV_{lim} values in combination with P2 and P4 topologies;
- P4 topology's optimal EV_{lim} values decrease with increasing ICE downsizing level;
- The lowest sensitivity of all combinations is for P4 topology with $1.5\ TC$ concept, where the CO_2 results change only around one gCO_2/km.
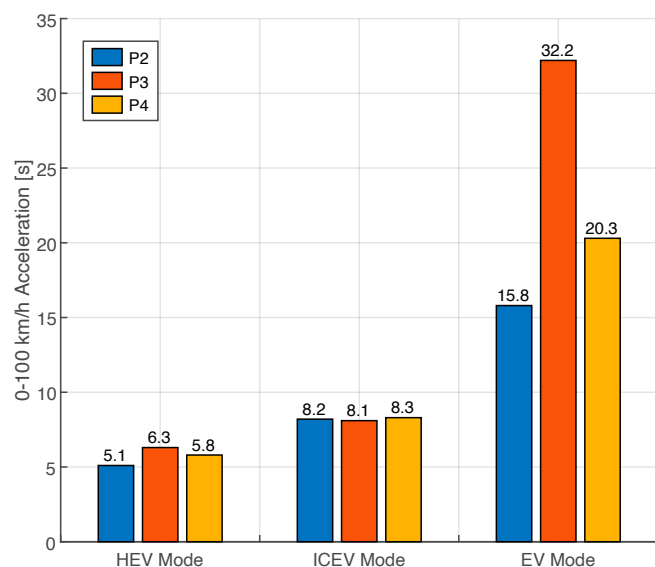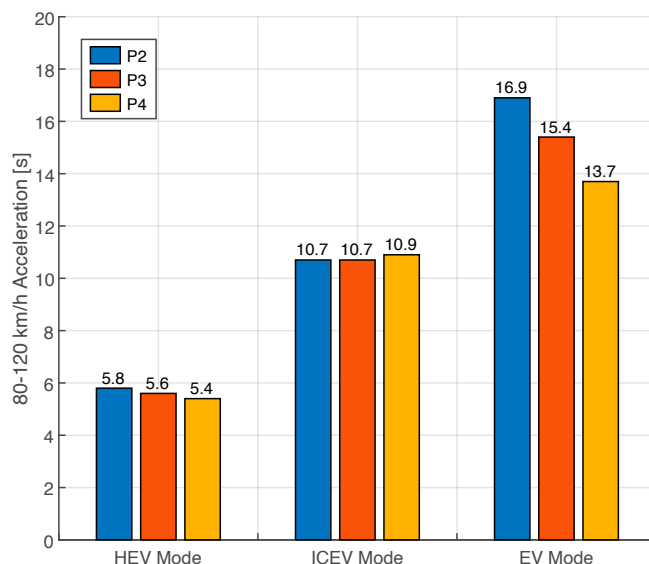
FIGURE 11: 80-120 km/h acceleration for $2.0\ NA$ concept and all HEV topologies, at 5th gear
OBRÁZEK 11: Zrychlení 80-120 km/h pro koncept motoru 2.0 NA a všechny HEV topologie, na 5. převodový stupeň

Finally, for some combinations, the EV_{lim} optimization can bring up to 5 gCO_2/km potential.

4.6. OVERALL VEHICLE DYNAMICS RESULTS

We have prepared several vehicle dynamics scenarios to compare the different hybridization variants: acceleration of 0-100 km/h, 60-80 km/h, 60-100 km/h, and 80-120 km/h, and the maximum vehicle speed simulation. We have simulated all HEV powertrain and ICE concept combination; however, here we present only the

FIGURE 10: 0-100 km/h acceleration for $2.0\ NA$ concept and all HEV topologies
OBRÁZEK 10: Zrychlení 0-100 km/h pro koncept motoru $2.0\ NA$ a všechny HEV topologie

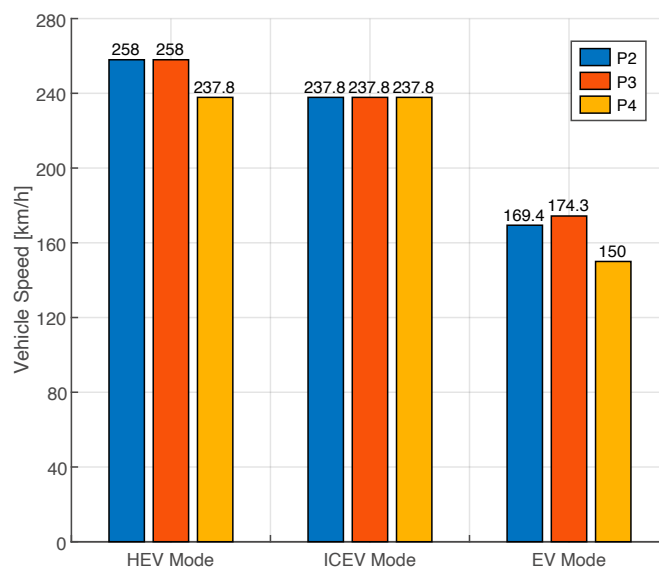**FIGURE 12:** Maximum vehicle speed for $2.0\ NA$ concept and all HEV topologies in different driving modes
OBRÁZEK 12: Maximální rychlost vozidla pro koncept motoru 2.0 NA a všechny HEV topologie a jízdní módy

Evaluation of Plug-in Parallel HEV Topologies Using Optimal Control Methods and Vehicle Dynamics Simulation
RASTISLAV TOMAN, JOLANA HEŘMANOVÁ

MECCA   02 2020   PAGE 32

2.0 NA concept results, as the map-based approach does not capture well the dynamic effects of turbocharged ICE concepts *1.0 TC*, and *1.5 TC* – as it was discussed in chapter 3.1. The P2, P3, and P4 topologies are compared in three different modes: hybrid (HEV), conventional (ICEV), and pure electric (EV).

4.6.1 ACCELERATION RESULTS

The acceleration tests consist of 0-100 km/h acceleration, and then the tests of 60-80 km/h, 60-100 km/h, and 80-120 km/h accelerations at the 5th and 6th gear, for all driving modes (HEV, ICEV, EV). The gear shifting strategy for 0-100 km/h acceleration considers the maximum ICE or EM speed. All acceleration results are listed in table 6, and shown in figures 10, and 11.

The P2 topology achieves the best 0-100 km/h acceleration in combined HEV mode, followed by the P4, and P3 topologies (figure 10). The case of EV acceleration shows the same order in topologies' performance: the best result is achieved by the P2, followed by P4, and finally P3. The ICEV 0-100 km/h accelerations are the only accelerations, where the variation is very low: all achieve results around 8.2 seconds. The HEV and EV results are strongly influenced by the gear ratios available for the EM: the P2 topology can shift gears, whereas the P3, and P4 can only make use of single gear, which is more beneficial for P4. Finally, the EV accelerations are logically also limited by the maximum EM power.

The rest of the table 6 contains the other accelerations at constant gear: sensitivities 60-80 km/h, 60-100 km/h, and 80-120 km/h, both on 5th gear, and 6th gear; all for *2.0 NA* engine concept. The 80-120 km/h scenario at 5th gear is shown in figure 11.

Also, these results are influenced mostly by the total gear ratios for different machines (ICE, EM): the P4 topology performs consistently as the best for both the HEV and EV acceleration modes, and P2 as the worst; the ICEV accelerations show very little sensitivity, because the only differences are the drivetrain efficiencies, and vehicle masses. The biggest variation happens again in case of EV acceleration mode, as the topologies vary greatly in their final gear ratios.

The 6th gear acceleration modes are qualitatively the same as on 5th gear.

4.6.2 MAXIMUM VEHICLE SPEED

The final test is the vehicle maximum speed, which depends mainly on the maximum total powertrain power, available for different driving modes (figure 12). The combined HEV maximum speed is transmission range limited and exceeds the vehicle speeds of 250 km/h for both the P2 and P3 topology. The P4 maximum HEV speed is in this case the same as for ICEV driving mode, due to P4 electric motor speed limit, as the EM is declutched above 150 km/h, and therefore not

providing power. The ICEV maximum speeds are all around 238 km/h.

Finally, the maximum achievable EV speeds are all limited by the EM maximum power of 54 kW, the P3 performing better then P2 topology. P4 maximum EV speed is also limited by abovementioned EM speed limit, that is bound to the rear axle gear ratio design.

5. CONCLUSIONS

Our paper presents a full development and benchmarking methodology for HEV powertrains, that is built on GT-Suite simulation software platform. The methodology consists of a combination of vehicle CO_2 homologation simulations (using WLTP methodology), and some vehicle dynamics tasks (different accelerations test, and maximum vehicle speed test).

We have prepared HEV simulation models using two different simulation approaches: a backward-kinematic approach (KIN models), and a dynamic approach (DYN models). Our KIN models are combined with GT-Suite's built-in optimal energy management control methods ECMS and Dynamic Programming (DP). Both KIN and DYN models were then used for the CO_2 WLTP homologation studies, obtaining Charge Sustaining (CS) CO_2, and All Electric Range (AER) results, together with the already mentioned additional vehicle dynamics results.

The whole presented methodology was tested on three different HEV topologies (P2, P3, and P4) in combination with three different ICE concepts (*2.0 NA*, *1.5 TC*, and *1.0 TC*), at the same hybridization level (with P_{ICE} of 135 kW and P_{EM} of 54 kW), using a six-speed transmissions, for a C-class plug-in HEV with a 14.8 kWh high voltage battery. All combinations show very good results compared to conventional powertrain, either in CO_2 homologation tests, or in vehicle dynamics tests:

- ICEV comparison of the three ICE concepts with different downsizing levels reveal a well-known fact, that downsized engines perform better in homologation driving cycles, such as WLTC;
- Total CO_2 reduction potentials from ICEV to PHEV homologation CO_2 values are similar for all powertrains, ranging from -95 to -119 gCO_2/km;
- The first part of the homologation are the AER tests, that show greater potentials for P4 and P2 HEV variants, since these use the EM in a more efficient manner, reaching AER values of ~66.7 km (P4), ~62.3 km (P2). However, the P3 also achieves high AER values of ~54.9 km;
- The second part of the homologation are the CS tests, where the different HEV powertrain combinations

Evaluation of Plug-in Parallel HEV Topologies Using Optimal Control Methods and Vehicle Dynamics Simulation
RASTISLAV TOMAN, JOLANA HEŘMANOVÁ

MECCA 02 2020 PAGE 33

reach CO_2 reduction potentials from -22 to -45 gCO_2/km (using DP control method);

- The P4 powertrains perform the best in the CS tests, together with the *2.0 NA* ICE concept – on the other end of the results were the P2 topology, and the *1.5 TC* concept;
- The P2 topology CS results can be further improved by the gear shifting strategy optimization: bringing additional ~5-10 gCO_2/km improvement, beating the abovementioned P4 results;
- The vehicle 0-100 km/h acceleration tests show the biggest performance benefit for P2 – that shifts gears also for the EM – followed by the P4, and then P3;
- The P4 topology then performs best at constant gear vehicle acceleration tests, followed by the P3, and P2.

There are three main conclusions from the PHEV homologation and vehicle dynamics studies:

1. There is no synergy effect between the powertrain hybridization and ICE downsizing, the trend seems to be rather opposite: *2.0 NA* concept is reaching the highest CO_2 reduction potentials;
2. It is valuable to optimize the HEV topology having the ICE concept in mind; however, the current PHEV homologation favors the AER, which may discourage developments in this area: the "simple" addition of a large enough battery (with AER of 50 km), reduces the homologation CO_2 by 90 gCO_2/km or more;
3. The vehicle dynamics tests further stress the importance of holistic HEV powertrain optimization: especially the transmissions gear ratios, with the goal of getting the best also out of the EM operation.

Apart from the overall homologation CO_2 and vehicle dynamics studies, we have also tested the performance of the GT-Suite's implementations of ECMS and DP optimal control methods:

- DP control method is generally more computationally demanding, but offers a user advantage of not having to calibrate for a correct equivalence factor to reach a CS cycle condition, as for the ECMS method;
- Rather surprising result of the comparison of these two control methods in GT-Suite is, that in some cases the ECMS can reach values closer to the theoretical global optimum compared to DP method, which is "advertised" as the globally optimal control method;
- However, both methods are consistent, providing qualitatively the same results, showing similar trends;
- Both methods are sensitive on their settings: in the case of DP it is the discretization of control inputs, and of state variable; ECMS is sensitive on the equivalence factor;
- Additional heuristic parameters help ensure the CS convergence of ECMS method and can further improve the CO_2 results.

Our further work will focus mainly on two areas: first is the amplification of the HEV model database – adding more HEV topologies; and second, embedding our simulation methodology into a multi-parametric and multi-objective HEV powertrain optimization strategy.

ACKNOWLEDGEMENTS

LIST OF NOTATIONS AND ABBREVIATIONS

AER	All Electric Range
AWD	All-wheel drive
BSFC	Brake-specific fuel consumption
CAE	Computer Aided Engineering
CD	Charge Depleting
CO_2	Carbon dioxide
CS	Charge Sustaining
DP	Dynamic Programming
DYN	Dynamic model
ECMS	Equivalent Consumption Minimization Strategy
ECU	Engine Control Unit
EM	Electric motor
EV	Electric Vehicle
FC	Fuel Consumption
FWD	Front-wheel drive
GT	Gamma Technologies
HEV	Hybrid electric vehicle
HV	High voltage
ICE	Internal combustion engine
ICEV	Internal Combustion Engine Vehicle
KIN	Kinematic model
LPS	Load Point Shifting
NA	Naturally aspirated
OEM	Original Equipment Manufacturer
OVC-HEV	Off-Vehicle Charging Hybrid Electric Vehicle
PHEV	Plug-In Hybrid Electric Vehicle
PMP	Pontryagin's minimum principle
RDE	Real Driving Emissions
RPM	Revolutions per minute
SOC	State of Charge
TC	Turbocharged
UF	Utility Factor

Evaluation of Plug-in Parallel HEV Topologies Using Optimal Control Methods and Vehicle Dynamics Simulation
RASTISLAV TOMAN, JOLANA HEŘMANOVÁ

MECCA 02 2020 PAGE 34

VVT	Variable valve timing
WLTC	Worldwide Harmonized Light-Duty Vehicles Test Cycle
WLTP	Worldwide Harmonized Light-Duty Vehicles Test Procedure

REFERENCES

[1] Reducing CO_2 emissions from passenger cars. European Commission, online, cited: 2019-06-31, accessed from: https://ec.europa.eu/clima/policies/transport/vehicles/cars_en

[2] Sundström, O., Guzzella, L., Soltic, P. (2008). Optimal Hybridization in Two Parallel Hybrid Electric Vehicles using Dynamic Programming, IFAC Proceedings Volumes, 41, 2: 4642-4647

[3] Lodaya, D., Zeman, J., Okarmus, M., Mohon, S., et al. (2020). Optimization of Fuel Economy Using Optimal Controls on Regulatory and Real-World Driving Cycles, SAE Int. J. Advances & Curr. Prac. in Mobility 2(3):1705-1716, 2020, doi:10.4271/2020-01-1007.

[4] Guzzela, L., Sciaretta, A. Vehicle Propulsion Systems: Introduction to Modelling and Optimization, Springer, 2013, ISBN 978-3-642-35913-2

[5] Biasini, R., Onori, S., Rizzoni, G. (2013). A near--optimal rule-based energy management strategy for medium duty hybrid truck, Int. J. Powertrains, Vol. 2, Nos. 2/3: 232-261

[6] Zhou, H., Xu, Z., Liu, L., Liu, D., Zhang, L. (2018). A Rule--Based Energy Management Strategy Based on Dynamic Programming for Hydraulic Hybrid Vehicles, Hindawi – Mathematical Problems in Engineering, Vol. 2018, doi:10.1155/2018/9492026

[7] Shen, W., Yu, H., Hu, Y., Xi, J. (2016). Optimization of Shift Schedule for Hybrid Electric Vehicle with Automated Manual Transmission, Energies 2016, 9, 220, doi:10.3390/en9030220

[8] Wang, R., Lukic, S. (2012) Dynamic Programming Technique in Hybrid Electric Vehicle Optimization, IEEE Xplore, doi: 10.1109/IEVC.2012.6183284

[9] Zeng, Y., Sheng, J., Ming, L. (2018). Adaptive Real-Time Energy Management Strategy for Plug-In Hybrid Electric Vehicle Based on Simplified-ECMS and a Novel Driving Pattern Recognition Method, Mathematical Problems in Engineering, p. 1-12, doi:10.1155/2018/5816861

[10] Nüesch, T., Cerofolini, A., Mancini, G., Cavina, N., Onder, Ch., Guzzella, L. (2014). Equivalent Consumption Minimization Strategy for Control of Real Driving NOx Emissions of a Diesel Hybrid Electric Vehicle, In: Energies 2014, vol. 7, p. 3148-3178, doi:10.3390/en70532148

[11] Yuan, Z., Teng, L., Fengchun, S., Peng, H. (2013). Comparative Study of Dynamic Programming and Pontryagin's Minimum Principle on Energy Management for a Parallel Hybrid Electric Vehicle, Energies 2013, 6, 2305-2318, doi:10.3390/en6042305

[12] Zeman, J., Papadimitriou, I., Watanabe, K., Kubo, M., Kumagai, T. (2012). Modeling and Optimization of Plug-In Hybrid Electric Vehicle Fuel Economy, SAE Technical Paper 2012-01-1018, doi:10.4271/2012-01-1018

[13] Bellman, R. (1966). Dynamic Programming, Science, vol. 153, no. 3731, pp. 34-37.

[14] UN Global Technical Regulation No. 15: Worldwide harmonized Light vehicles Test Procedure (ECE/TRANS/180/Add.15). United Nations Economic Commission for Europe, 2019-06-26, cited: 2020-11-01, accessed from: https://www.unece.org/fileadmin/DAM/trans/main/wp29/wp29wgs/wp29gen/wp29registry/ECE-TRANS-180a15am5e.pdf

Evaluation of Plug-in Parallel HEV Topologies Using Optimal Control Methods and Vehicle Dynamics Simulation
RASTISLAV TOMAN, JOLANA HEŘMANOVÁ

MECCA 02 2020 PAGE 35

SUBSCRIPTION INFORMATION
FOR YEAR 2020

MECCA IS PUBLISHED THREE TIMES A YEAR

* Middle European countries profit special price .... 200 CZK
  (in Czech crowns) without shipping costs per issue.
* Price for rest of world ....15 €
  per issue without shipping costs.
* Price for annual subscription including shipping costs for Czech republic .... 760 CZK
* Price for annual subscription including shipping costs for other middle European countries................................. 860 CZK
* Price for annual subscription including shipping costs for the rest of Europe ....56 €
* Price for annual subscription including shipping costs for the overseas...60 €

PLEASE PAY THE AMOUNT ON THE FOLLOWING BANK ACCOUNT:

Company legal name: Czech Technical University in Prague
                                Faculty of Mechanical Engineering

Company full address: Technická 4
                                16607 Praha 6
                                Czech Republic

Account number: 19-5505030267
Bank code: 0100
Bank name: Commercial bank (KB)
Full bank address   Dejvická 52, 160 59 Praha 6
IBAN CODE (mandatory):   CZ4201000000195505030267
SWIFT CODE (mandatory):   KOMBCZPPXXX

FOR ALL QUESTIONS, PLEASE, CONTACT THE EDITOR:

Gabriela Achtenová
Czech Technical University in Prague
Technická 4, 166 07 Praha 6
Czech Republic
Tel.: +420 224 352 499, Fax: +420 224 352 500
mecca@fs.cvut.cz
gabriela.achtenova@fs.cvut.cz

LIST OF COUNTRIES PROFITING THE SPECIAL PRICE OF MECCA:

Czech Republic, Slovakia, Poland, Hungary, Romania, Bulgaria, Former USSR republics, Former Yugoslav republics

GUIDELINES FOR AUTHORS

A. LANGUAGE
01) Language of paper – American English
02) Abstract, captions and keywords will be bilingual English and Czech, optionally English and Slovak. Authors from the Czech and Slovak Republic should prepare abstract, keywords and captions in English and native language. The abstract and captions for other authors will be translated by the publisher to Czech language.

B. LENGTH
Title   should not exceed 10 words
Subtitle   should not exceed 15 words
Abstract   should not exceed 200 words
Paper   without limit

C. ORDER OF CONTENTS
01) Title
02) Author(s) name: per author company/institute, address, and e-mail (on new line)
03) Abstract
04) Keywords
05) Body of the paper. The paper should be divided into logical numbered sections.
06) Preferred structure:
– Introduction: Background – Motivation – Goals
– Used methods
– Results
– Analysis of results and evaluation
– Conclusion: Result Utilization – Prospects
07) Acknowledgements
08) List of notations and abbreviations (in alphabetical order)
09) References
10) Appendices: Long derivation of equations, description and parameters of experimental equipment or methods, etc.

To facilitate the blind reviewing process, the authors are asked provide on a separate first page the items 1) and 2) and to start the main part of the article with 1) Title; and then 3) Abstract, and so on.

D. GRAPHICAL ARRANGEMENT
Title: Times New Roman 17b, Bold
Body of paper, abstract, equation numbering: Times New Roman 11b. Titles of sections Times New Roman 12b Bold. Symbols of physical quantities used in text: italic. SI units, wherever possible. Combined units should be written with dot (example: N.m, m.s^{-2}, …). Authors should avoid the usage of footnotes.
Captions: Times New Roman 10b, in bold – number and caption, normal – text of legend. See examples:
Figure 1: This is a figure.
Table 1: This is a table.
All illustrations should be numbered sequentially with arabic numbers.
Equations: Times New Roman italic. Variable 12b, Index 7b, Small index 5b, Symbol 18b, Small symbol 12b. Mathematical operators and constants (Ex.: sin, e, π, …) Times New Roman 12b normal.

All equations should be numbered sequentially with arabic numbers. List of notations either under every equation, or at the end of paper – see paragraph D (according to number and content of equations). Long derivation as appendix on the end of paper.
References: References referred in text in square brackets in format of text (Ex: [1])
Format of references, examples:
[1] Author A., Author B. and Author C. (2002). This is journal article, In: Journal for Interesting Papers, Vol. 10, No. 3, p. 130–145. ISSN
[2] Author A., Author B. and Author C. (eds.). Our Book on Car Technology, MIT Press, Massachusetts, 2002, p. 23-145. ISBN
[3] Author A., Author B. and Author C. (2002). My paper in a conference, In: Editor A., Editor B. and Editor C. (eds.). Proceedings Of Our Meeting in a Far Away Exotic Place, MIT Press, Massachusetts, p. 78-89. ISBN

E. ILLUSTRATIONS
The Journal is full-color.
The authors are responsible for delivering high-quality graphic material. In the case of illustrations sent via mail, the orientation of illustrations should be indicated, as well as their number in the article. The illustrations sent electronically, should be sent in the correct orientation and in a resolution at least 300 dpi, in common graphical formats.

F. SUBMISSION OF MANUSCRIPTS
Text should be in all cases prepared in electronical form. Paper can be sent via mail (the contents of mail should be illustrations and diskette 3,5" or CD with text), or via e-mail on the address mentioned below.
Text should be sent in format MS Word 2000 or older (format doc, or rtf). Do not merge illustrations in the text to avoid excessive file size. All illustrations should be sent in separate files. No illustrations will be returned unless specifically requested.
Contact address for submission of paper:
ČVUT, FS, MECCA
Gabriela Achtenová
Technická 4, 166 07 Praha 6, Czech Republic
Tel.: +420 2 24 35 24 99, Fax: +420 2 24 35 25 00
E-mail: gabriela.achtenova@fs.cvut.cz

G. COPYRIGHT
The papers submitted to journal MECCA have not been previously published or submitted elsewhere. The copyright of accepted papers becomes the property of Czech Technical University, and usage of any part of papers without permission of Czech Technical University will be not allowed. Authors who wish to reproduce already published illustrations should asked the permission by the copyright holder. Authors are asked to sign copyright agreement.

H. PUBLICATION
All articles will be blind reviewed. The first author, if no other contact person is marked, will be informed about the decision as soon as possible.
Authors will get 3 copies of the journal in which the article is published.

MASTER OF AUTOMOTIVE ENGINEERING

ENTRANCE LEVEL: Technical bachelor (mechanical, transport, or electro engineering)

CTU
Prague
Czech republic

(E)

ITB
Bandung
Indonesia

(E), (I)

ENSTA
Brest
France

(F)

TUCH
Chemnitz
Germany

(G)

3rd SEMESTER

Entrance exam IFP

ENSTA
- Design
  of Vehicles
- Modelisation
  and Computation
(F)

HAN
Vehicle Dynamics
and Intelligent
Transport Systems

(E)

CTU
Advanced
Powertrains

(E)

TUCH
Alternative
Powertrains

(G)

IFP
Paris
France

(F)+(E)

4th SEMESTER devoted to final thesis and 5 months internship in an industrial or academic environment anywhere in the world

MASTER DEGREE IN AUTOMOTIVE ENGINEERING
Master degree from 2 countries with respect to chosen specialisation in 3rd semester

(F) – in French, (E) – in English, (I) – in Indonesian, (G) – in German

CTU
Czech Technical University in Prague
Czech Republic
Gabriela Achtenová
gabriela.achtenova@fs.cvut.cz
Tel.: +420 224 352 499

ITB
Institut Teknologi Bandung
Indonesia
Andi Isra Mahyuddin
aim@ftmd.itb.ac.id

ENSTA
ENSTA Bretagne
France
Yann Marco
yann.marco@ensta-bretagne.fr
Tel.: +33 298 348 844

TUCH
Technische Universität Chemnitz
Germany
Martin Hipp
martin.hipp@mb.tu-chemnitz.de
Tel.: +49 371 531 337 94

HAN
Hogeschool van Arnhem en Nijmegen
The Netherlands
Kea Bouwman
kea.bouwman@han.nl
Tel.: + 31 26 384 93 14

DEADLINE FOR EU AND NON EU STUDENTS 1st MAY 2021
For application form, detailed programme, studying conditions, tuition fees and all other informations, please see: www.emae.eu